haematologica
Journal of The Ferrata Storti Foundation

The new small tyrosine-kinase inhibitor ARQ531 targets acute myeloid leukemia cells by disrupting multiple tumor-addicted programs

by Debora Soncini, Stefania Orecchioni, Samantha Ruberti, Paola Minetto, Claudia Martinuzzi, Luca Agnelli, Katia Todoerti, Antonia Cagnetta, Maurizio Miglino, Marino Clavio, Paola Contini, Riccardo Varaldo, Micaela Bergamaschi, Fabio Guolo, Mario Passalacqua, Alessio Nencioni, Fiammetta Monacelli, Marco Gobbi, Antonino Neri, Giovanni Abbadessa, Sudharshan Eathiraj, Brian Schwartz, Francesco Bertolini, Roberto M. Lemoli, and Michele Cea

Haematologica 2019 [Epub ahead of print]

Debora Soncini, Stefania Orecchioni, Samantha Ruberti, Paola Minetto, Claudia Martinuzzi, Luca Agnelli, Katia Todoerti, Antonia Cagnetta, Maurizio Miglino, Marino Clavio, Paola Contini, Riccardo Varaldo, Micaela Bergamaschi, Fabio Guolo, Mario Passalacqua, Alessio Nencioni, Fiammetta Monacelli, Marco Gobbi, Antonino Neri, Giovanni Abbadessa, Sudharshan Eathiraj, Brian Schwartz, Francesco Bertolini, Roberto M. Lemoli, and Michele Cea.
The new small tyrosine-kinase inhibitor ARQ531 targets acute myeloid leukemia cells by disrupting multiple tumor-addicted programs.
Haematologica. 2019; 104:xxx
doi:10.3324/haematol.2019.224956

The new small tyrosine-kinase inhibitor ARQ531 targets acute myeloid leukemia cells by disrupting multiple tumor-addicted programs

Debora Soncini[1], Stefania Orecchioni[2], Samantha Ruberti[1], Paola Minetto[1,3], Claudia Martinuzzi[1], Luca Agnelli[4], Katia Todoerti [4], Antonia Cagnetta[1,3], Maurizio Miglino[1,3], Marino Clavio[1,3], Paola Contini[5], Riccardo Varaldo[6], Micaela Bergamaschi[1], Fabio Guolo[1], Mario Passalacqua[7], Alessio Nencioni[5], Fiammetta Monacelli [5], Marco Gobbi [1,3], Antonino Neri [4], Giovanni Abbadessa[8], Sudharshan Eathiraj [8], Brian Schwartz [8], Francesco Bertolini [2], Roberto M. Lemoli [1,3], Michele Cea [1,3]

[1] University of Genoa, Department of Internal Medicine and Specialities (DiMI), Chair of Hematology, Italy

[2] Laboratory of Hematology-Oncology European Institute of Oncology IRCCS, Milan, Italy

[3] IRCCS Ospedale Policlinico San Martino, Genoa, Italy

[4] Department of Oncology and Hemato-Oncology, University of Milan, Milan, Italy

[5] University of Genoa, Department of Internal Medicine and Specialities (DiMI), Italy

[6] Division of Hematology and Hematopoietic Stem Cell Transplantation Unit, Ospedale Policlinico San Martino, Genoa, Italy

[7] University of Genoa, Department of Experimental Medicine (DIMES), Italy

[8]ArQule, One Wall Street, Burlington, MA, USA

Corresponding Author

Michele Cea, MD,

Department of Internal Medicine and Specialities (DiMI), University of Genoa,

Viale Benedetto XV n.6

16132 Genoa, Italy.

Phone: 39-010-353-7970;

Fax: 39-010-353-38701;

E-mail: michele.cea@unige.it

Conflict of Interest:

E.S., A.G. and S.B. are current or former employees and shareholders of ArQule Inc. All other authors declare no competing financial interests.

Running Title: Preclinical activity of ARQ531 in Acute Myeloid Leukemia

Abstract words: 198

Text words: 3887

Number of Figures: 7

Number of Tabs: 1

References: 61

ABSTRACT

Tyrosine kinases have been implicated in promoting tumorigenesis of several human cancers. Exploiting these vulnerabilities has been shown to be an effective anti-tumor strategy as demonstrated for example by the Bruton's tyrosine kinase (BTK) inhibitor, ibrutinib, for treatment of various blood cancers. Here, we characterize a new multiple kinase inhibitor, ARQ531, and evaluate its mechanism of action in preclinical models of acute myeloid leukemia. Treatment with ARQ531, by producing global signaling pathway deregulation, resulted in impaired cell cycle progression and survival in a large panel of leukemia cell lines and patient-derived tumor cells, regardless of the specific genetic background and/or the presence of bone marrow stromal cells. RNA-seq analysis revealed that ARQ531 constrained tumor cell proliferation and survival through Bruton's tyrosine kinase and transcriptional program dysregulation, with proteasome-mediated MYB degradation and depletion of short-lived proteins that are crucial for tumor growth and survival, including ERK, MYC and MCL1. Finally, ARQ531 treatment was effective in a patient-derived leukemia mouse model with significant impairment of tumor progression and survival, at tolerated doses. These data justify the clinical development of ARQ531 as a promising targeted agent for the treatment of patients with acute myeloid leukemia.

INTRODUCTION

Acute myeloid leukemia (AML) is an aggressive disease characterized by uncontrolled clonal proliferation of abnormal myeloid progenitor cells in the bone marrow and blood. Despite recent advances in its treatment, as many as 70% of patients aged 65 or older will die within 1 year of diagnosis. Efficacy of standard high-dose chemotherapy and stem cell transplantation is limited by treatment-related morbidity and mortality, especially in elderly patients. (1-3) Cancer treatment is undergoing a significant revolution from “one-size-fits-all” cytotoxic therapies to tailored approaches that precisely target molecular alterations. Notably, precision medicine, by linking specific genetic anomalies of tumors with available targeted therapies, is emerging as an innovative approach for AML treatment, with development of breakthrough drugs targeting specific molecular features (e.g. FLT3 and IDH1/2 inhibitors). (4-6) However, identification of patients who will benefit from targeted therapies is more complex than simply identifying patients whose tumors harbor the targeted aberration. A rational combination of therapeutic agents may prevent the development of resistance to therapy, with molecular strategies aimed at targeting multiple pathways resulting in a more effective treatment across cancer subtypes.

The Bruton’s tyrosine kinase (BTK), a member of the TEC family kinases, is a critical terminal kinase enzyme in the B-cell antigen receptor (BCR) signaling pathway. (7, 8) Its activation leads to BTK phosphorylation which in turn results in downstream events such as proliferation, immune function alteration and survival through multiple signaling cascades. (9) Chronic activation of BTK-mediated signaling represents a key driver for a number types of cancers, (10-14) including AML. (15-22) Therefore, new inhibitors are needed to better target tyrosine kinases in these patients. Recent studies have shown that oncogenic cellular dysregulation is critical for the activity of the anti-BTK targeting

agent ibrutinib, (23, 24) and that co-treatment with BET protein bromodomain antagonists or BCL-2 inhibitors may enhance the efficacy of ibrutinib in tumor cells. (25, 26)

Herein, we characterize ARQ531, a reversible small molecule inhibitor of BTK and several additional kinases, in preclinical models of AML. We provide evidence that ARQ531 greatly compromises survival of AML cells by inducing a “one shot” inhibition of multiple oncogenic transcriptional pathways. This results in potent anti-AML activity in a patient-derived xenograft (PDX) AML mice model, providing rationale for future clinical trials.

METHODS

Reagents

ARQ531 was provided by ArQule, Inc (Burlington, MA). The compound was dissolved in DMSO (Sigma, Aldrich) and stored at 10mM at -80°C for experiments. Ibrutinib (IBR), daunorubicin (DNR), cytarabine (ARA-C) and MG132 were purchased from Selleck Chemicals LLC (Houston, TX). ZVAD-FMK was purchased from Promega (Cat.No G7232).

Patient-derived xenograft AML cells

Experiments were carried out on non-obese diabetic severe combined immunodeficient (NOD/SCID) interleukin-2 receptor g (IL-2Rg)–null (NSG) mice, 6 to 8-weeks-old. NSG mice were bred and housed under pathogen-free conditions in the animal facilities at the European Institute of Oncology–Italian Foundation for Cancer Research Institute of Molecular Oncology (IEO-IFOM, Milan, Italy). All animal experiments were carried out in strict accordance with the Italian laws (DLvo 26/2014 and following additions) and were approved by the institutional committee. NSG mice were engrafted with 300.000 primary human AML cells (M4, acute myelomonocytic leukemia with $FLT3^{wt}$). At day 19 post-graft, once a systemic xenograft was confirmed, mice were randomized into three groups: vehicle-treatment group (n=5), low-dose ARQ531 treatment group (25 mg/kg; n=5) and high-dose ARQ531 treatment group (37.5mg/kg; n = 5) and the percentage of human leukemic cells in peripheral blood was measured weekly till day 42. The phenotype of human cells in NSG mice was evaluated using the following anti-human antibodies: anti-CD117-PeCy7 (IMMU 103.44), -CD45-APC (J.33), -CD34-APC-Cy7 (D3HL60.251) from Beckman-Coulter (Irving, TX, USA) and anti-mouse CD45-PE (30-F11) from BD Biosciences to exclude murine cells contamination. Cell suspensions were evaluated by a 3-laser, 10-colour flow cytometer (Navios, Beckman Coulter, Brea, CA, USA) using analysis gates designed to exclude dead cells, platelets, and debris. Percentages of stained cells were determined and

compared to appropriate negative controls. Seven-aminoactinomycin D (7AAD) from Sigma-Aldrich was used to enumerate viable, apoptotic, and dead cells.

Statistical analyses

All in vitro experiments were repeated at least three times and performed in triplicate; a representative experiment is shown in each figure. All data are shown as mean ± standard deviation (SD). The Student's t test was used to compare two experimental groups using Graph-Pad Prism software (http://www.graphpad.com). The minimal level of significance was specified as $p<0.05$. Survival analysis was performed by the Kaplan-Meier method, and the log-rank test was used to compare survival differences. Drug interaction were assessed by CalcuSyn 2 software (Biosoft), which is based on the Chou-Talalay method. Combination Index (CI) = 1, indicates additive effect; CI<1 indicates synergism; CI>1 indicates antagonism.

RESULTS

ARQ 531 shows strong anti-AML activity but preserves normal hematopoietic stem cells (HSCs).

In line with previously reported data, (15, 16) we observed that BTK is frequently dysregulated in AML, with mRNA levels significantly higher than in other cancer types. (**Suppl. Fig. S1**) To confirm its relative abundance, we screened a representative panel of human AML cell lines and primary blasts for BTK expression and activity by western blot. (**Fig.1A**) Protein was detectable in all AML-screened cells (15/15) and, more importantly, independent of specific mutational profiling. Similarly, BTK activity (measured by Y223 phosphorylation) was observed in FLT3 wild-type and FLT3 mutants as well. An analogous investigation was applied to a larger cohort of AML patients derived from The Cancer Genome Atlas (TCGA) database, which showed uniform expression of BTK transcript in different AML subtypes. Overall, these data, by confirming BTK presence in AML, support its targeting in this hematologic malignancy, as previously reported. (14, 15)

ARQ531 is a recently described reversible BTK inhibitor with promising activity in mouse models of CLL and lymphomas. (27) Based on constitutively active BTK levels observed in AML cells, we evaluated the therapeutic activity of ARQ531 on these cells, using ibrutinib as a control. In-vitro efficacy screening was performed on cultured (n=8) and primary (n=13) AML cells, comparing the efficacy of both drugs. As shown in **Figure 1B**, ARQ531 exposure reduced in vitro viability more than ibrutinib (**Fig.1C**). IC_{50} analysis at 48 hours after treatment showed greater sensitivity to ARQ531 compared with ibrutinib, which exhibited 10-fold lower activity. (**Fig.1D**) A significant anti-AML effect of ARQ531 was also observed on blasts from AML patients (n=13) regardless of mutational status, European leukemia Net (ELN) risk, and surface expression of CD117. (**Fig.1E; Tab.1**) Consistent with these data, a dose-dependent increase in the percentage of apoptotic and dead cells measured by Annexin V and Propidium iodide staining was also observed after ARQ531 treatment,

together with several apoptotic features including caspase 3 and poly (AD-ribose) polymerase cleavage as well as reduction of anti-apoptotic MCL-1 and BCL-2 protein expression. (**Fig.1F-G** and **Suppl. Fig.S2A**) Viability was completely restored by pan-caspase inhibitor Z-VAD pre-incubation (**Suppl. Fig.S2B**) In contrast, ibrutinib treatment resulted in weaker effects on apoptosis, thus suggesting that ARQ531 is more effective than ibrutinib probably because it induces downregulation of additional survival mechanisms.

It is well known that the bone marrow microenvironment has a role in the promotion of tumor growth, survival and drug-resistance. (28) Therefore we treated AML cells in the presence of normal or leukemic mesenchymal stromal cells (MSCs). As expected, normal- and AML-stroma both protected tumor cells from spontaneous apoptosis, however ARQ531 efficacy was preserved, with no significant effect on the viability of MSCs (data not shown). Indeed, compared to spontaneous apoptosis of blast cells, ARQ531 increased cell death in AML cells cultured alone, and preserved its activity in the presence of normal or AML MSCs, suggesting that ARQ531 abrogates the survival benefit from stromal cells. (**Fig.2A**) Overall, our data indicate that ARQ531 is a potent anti-AML drug even in the presence of a tumor supportive microenvironment, and irrespective of FLT3 mutational status. (21) Finally, ARQ531 activity on normal cells was also investigated by employing clonogenic and viability assays in order to measure the impact of treatment on both $CD34^+$ cells and mononuclear cells isolated from the bone marrow and peripheral blood of healthy donors. As shown in **Figure 2 B-D**, all of these cells were largely unaffected by ARQ531 exposure at dose levels toxic to tumor cells, proving that ARQ531 targets cancer cells without off-target effects on HSCs, resulting in a favorable therapeutic index.

BTK signaling inhibition partially contributes to anti-AML activity of ARQ531

Based on its reported activity, we first studied the effect of ARQ531 on BTK-signaling by analyzing tumor cell migration. (27, 29-31). A transwell assay system was employed to investigate SDF-1/CXCR4 axis in ARQ531 anti-AML activity. As shown in **Supplementary Figure S3**, ARQ531 reduced tumor cell migration in response to stromal cell-derived factor 1 (SDF1) by 66% ($P = 0.001$), suggesting similar activity to ibrutinib (71% reduction; $P < 0.001$).

Next, to confirm the role of BTK in ARQ531 anti-AML activity, we investigated its effect on BTK-signaling in AML cells over a range of concentrations. As shown in **Figure 2E**, ARQ531 treatment completely abrogated BTK activity as measured by Y223 phosphorylation, similar to the effects seen with ibrutinib treatment. However, as seen in **Figure 1B**, ARQ531 has anti-AML activity even on BTK-low expressing cells, suggesting that BTK targeting might not be critical for ARQ531 activity. To corroborate this hypothesis, we treated BTK-silenced (BTK knocked down, BTK-KD) AML cells with increasing doses of ARQ531. ARQ531 treatment reduced viability of both BTK-KD and BTK wild-type cells to about 50% of control, demonstrating the importance of alternative targets for ARQ531 activity in AML. (**Fig.2F**)

ARQ531 treatment suppresses transcriptional oncogenic activity in AML cells

To identify ARQ531-induced global perturbations in transcriptional profiling, we generated RNA-Seq data and performed functional annotation analysis of drug- versus DMSO-treated AML cells. As shown in **Supplementary Figure S4A**, principal component analysis (PCA) segregated samples based on treatment suggest a coherent transcriptional result rather than global, non-specific transcriptional silencing in response to this drug. Indeed, differential expression analysis identified 377 and 852 genes that were significantly up-regulated and down-regulated, respectively, with a ratio greater than 2-fold and P value <0.05. (**Fig.3A, B**) As a measure of the specificity of this effect, GSEA analysis was performed on the entire set of signatures available from the Molecular Signatures Database (MSigDB).

Biological modules associated with oncogenic transcriptional programs (e.g., ribosomal biogenesis and assembly, UPR stress and MYC) were significantly enriched in ARQ531-suppressed genes. (**Fig.3C** and **Suppl. Fig.S4B**) In line with these findings, although treatment did not exert significant suppression of gene sets for factors linked to pathophysiology of AML, such as C/EBPα-β, RUNX1, PU.1, ERG and FLI1, a significant reverse correlation was observed for transcriptional signatures of MYC-upregulated target genes, which in turn reflects the selective suppression of its transcriptional networks. (**Fig.3D**) Indeed, RT-PCR analysis of MYC and its target, CDC2, showed consistent downregulation following short-term exposure to the drug, (**Suppl. Fig. S4C**) pointing to ARQ531 as a selective suppressor of the MYC-regulated transcriptional pathway. To further support these data, we used ARQ531-expression signature to query the Library of Integrated Network-Based Cellular Signatures (LINCS) Program (www.lincscloud.org, web interface available at http://amp.pharm.mssm.edu/L1000CDS2/#/index). As shown in **Figure 3E**, the most significant ARQ531-correlated signatures were represented by those of oncogenic transcription factor inhibitors (such as fluvastatin, gefitinib and HDAC inhibitors) as well as those related to knockdown of ribosome subunits and translation initiation factors. Together, these data indicate that ARQ531 inhibits oncogenic transcriptional pathways in AML cells.

ARQ531 interferes with the pro-survival MAPK pathway in OCI-AML3 cells

As already reported, ARQ531 is a potent, ATP-competitive, reversible inhibitor of BTK and several additional kinases important to the viability, proliferation, activation, and motility of tumor cells. (27) Among the most intriguing additional targets of ARQ531 are RAF1 and MEK1, constituents of the ERK signaling pathway that is frequently dysregulated in tumor cells. (32-34) To confirm this activity in AML, cells were treated with increasing doses of ARQ531. As expected, activation of AKT and ERK was inhibited in a dose-dependent manner, likely due to predicted inhibition of RAF1 and MEK1.

(**Fig. 4A**) Subsequent experiments confirmed this hypothesis by revealing specific impairment of these kinases after ARQ531 treatment. (**Fig. 4B**) To support the pivotal role played by ERK, we exposed cells to the mitogenic effects of higher serum concentration (20%). As shown in **Supplementary Figure S5 A-B**, this strategy resulted in enhanced phosphorylation of ERK, which rescued the anti-AML activity of this drug, thus providing evidence of ERK relevance in the observed anti-tumor effect. Moreover, consistent with RNA-Seq analysis, drug exposure resulted in prominent and specific downregulation of the oncogenic transcription factor MYC at the protein level. (**Fig. 4B**) Since the MAPK pathway enhances MYC protein stability by inducing its phosphorylation at serine 62, (35) we assessed p-MYC S62 changes in AML-treated cells. As shown in **Figure 4C**, ARQ531 exposure resulted in a prompt decrease of phosphorylation, followed by reduction of MYC protein. Accordingly, numerous MYC-addicted oncogenic cellular pathways, such as protein folding machinery, metabolic dependency and genome integrity, were compromised following this treatment, as highlighted by phospho-eukaryotic translation initiation factor 4E (eIF4e), ASCT2 and GLUT1 downregulation and γH2AX enhancement, respectively. (**Fig. 4D**) Combined drug screening revealed synergistic activity of ARQ531 with compounds affecting these programs, such as DNA damaging agents. (**Suppl. Fig. S6 A-B**) Overall, these data support the existence of a mechanism of action that begins with MAPK signaling dysregulation and results in ARQ531-induced cytotoxicity in AML cells. Among MYC-controlled programs, protein synthesis is emerging as the limiting step for tumor cell growth, (36) so we focused on this pathway. As shown in Figure 4D, AML cells treated with ARQ531 showed marked increases of eukaryotic translation initiation factor 4E-binding protein (4EBP1) with concomitant de-phosphorylation of p70 ribosomal S6 kinase (p70-S6K) and eIF4e which result in blocking of mRNA recruitment to ribosomes for protein translation. (37) These data suggest that ARQ531 is a modulator

of several hubs controlling translation initiation in AML cells, providing evidence of marked protein synthesis inhibition specifically triggered by this treatment.

Although *MYC* activation resulting from multiple tumor-driven genetic aberrations has been recognized as a major factor of leukemogenesis, its targeting did not show significant clinical benefit in AML. Thus, by using small interference RNA strategy (siRNA), we investigated the role of MYC in anti-AML activity of ARQ531. As shown in **Figure 4E**, *MYC*-silenced HL-60 cells (*MYC* knocked down, KD) were treated with increasing doses of ARQ531. Surprisingly, despite their sensitivity to this treatment, cells were quite resistant to the loss of MYC protein expression, indicating that additional targets are implicated in anti-AML activity of this small molecule.

Modulation of transcriptional regulatory machinery is an innovative strategy to treat AML. (38, 39) The oncogenic driver MYB, which is essential in hematopoiesis, is now emerging as a new target for anti-AML therapies. (40-45) We hypothesized that ARQ531 treatment of AML cells may inhibit this pathway. To validate this hypothesis, we measured MYB protein levels in ARQ531-treated cells. ARQ531 exposure resulted in marked MYB deregulation, (**Fig. 4F)** suggesting an important contribution to ARQ531 anti-tumor activity. To gain further insights into MYB reduction triggered by ARQ531, we tested proteasome contribution, as previously reported for other MYB-targeting agents. (43) As shown in **Figure 4G**, co-treatment with the proteasome inhibitor MG132 preserved MYB protein levels, suggesting that, in addition to its supposed effects on protein synthesis, ARQ531 affects MYB degradation. Therefore, our findings suggest that ARQ531 interferes with many pro-survival pathways, such as MAPK, in AML cells.

ARQ531 dysregulates multiple oncogenic transcription factors in AML cells

To gain insights into the molecular mechanisms of ARQ531, we analyzed treated HL-60 cells over time. As shown in **Figure 5A**, BTK signaling deregulation occurred early, after 2 hours of treatment,

followed by MYC downregulation. Importantly, apoptotic cell features, including PARP and caspase 3 cleavage, were seen after MYB decrease, suggesting these events are crucial for ARQ531 anti-tumor activity. Published data show that small molecule BET inhibitors, by downregulating hematopoietic transcription factors, lead to potent therapeutic effects in several cancer models, including AML. (46, 47) Therefore, we tested the anti-AML activity of the BTK inhibitor ibrutinib combined with the BET bromodomain inhibitor JQ1. (48) As was seen in other cell types, (25) the BET inhibitor enhanced the anti-tumor activity of the BTK inhibitor. (**Fig. 5B**) Western blot analysis of AML-treated cells confirmed these findings, further supporting the pivotal role of transcription factor deregulation in ARQ531 anti-AML activity. (**Fig. 5C**) Based on these data, we investigated the role of MYB in ARQ531 anti-AML activity by challenging BTK-silenced cells with the repurposed drug mebendazole, recently described as drug that induces MYB degradation. (44) As expected, mebendazole reduced cell viability of BTK-depleted cells more than control. (**Suppl. Fig. S7A**) We then performed several genetic studies to confirm these findings. As shown in **Figure 6A**, reduced viability was observed in MYC/MYB depleted cells compared with control, but more importantly, viability was significantly dampened in triple MYB/MYC/BTK silenced cells (reduction by 64.7% to 38.5%), suggesting that such inhibition is detrimental to AML cells. Consistently, simultaneous silencing of MYC, MYB and BTK resulted in PARP cleavage together with impairment of ERK phosphorylation. (**Fig. 6B**) Similar data were observed in BTK-KD cells. (**Fig. 6C** and **Suppl. Fig. S7B**) Nonetheless, the effect of triple knockdown was not quite equal to that of ARQ531 treatment, suggesting that other covalent or noncovalent targets are involved in its mechanism of action.

Since MYB is reported to be crucial for leukemogenesis, (42, 49) we assessed the relationship between BTK and MYB in AML cells. Molecular data analysis of different publicly available AML cohort databases revealed higher expression of BTK and MYB in AML cells compared to normal HSCs, with

a positive correlation. (**Suppl. Fig. S8 A-C**) These data support the notion that several oncogenic pathways, including BTK, MYB and MYC, are essential for leukemia cells maintenance, supporting ARQ531 as an effective multi-targeted agent for the treatment of AML.

ARQ531 shows potent activity in a patient derived (PDX) AML mouse model

Based on in-vitro data, we next assessed whether ARQ531 treatment would be effective and tolerable in animal models by using our established AML patient-derived xenograft (PDX) model. NSG mice (n=20) were engrafted with 300.000 primary human AML cells (M4, acute myelomonocytic leukemia). Successful engraftment was documented by measuring circulating human CD45+ cells in mice peripheral blood with flow cytometry weekly for 2 months. At day 19 post-graft, once a systemic xenograft was confirmed, mice were dosed orally with vehicle or ARQ531 (25 or 37.5 mg/kg; 5 mice/each group) daily for 2 weeks. Percentage of human cells in peripheral blood samples was measured once a week up to day 42. (**Fig. 7A**) ARQ531-treated mice had significant reduction in hCD45+ cell numbers despite very rapid growth of the aggressive leukemic cells. (**Fig. 7B**) At day 42 from treatment start, there were 66.5±0.1% and 69.5±0.2 % hCD45+ cells after ARQ531-treatment at 37.5 and 25 mg/kg, respectively; in contrast, vehicle-treated mice had 85% hCD45+ cells (** $0.005 < P < 0.008$; **Fig. 7C**). Also bone marrow and spleen analyses showed tumor burden (hCD45+) reduction, although it was not statistically significant. (**Suppl. Fig. S9**) In addition, ARQ531 treatment was found to significantly improve mouse survival. As shown in **Figure 7D**, Kaplan-Meier analyses indicated that ARQ531-treated mice, at higher dose, survived significantly longer than those treated with vehicle-control ($p<0.001$). Overall, treatment was well tolerated as suggested by the maintenance of body weight and the lack of signs of toxicity, such as lethargy, ruffled fur, respiratory distress and hunchback posture (data not shown). Together these data indicate that in vivo ARQ531 administration was well

tolerated and efficiently reduced leukemia cell growth, providing impetus for clinical evaluation of this novel small molecule.

DISCUSSION

AML cells often demonstrate constitutive activation of tyrosine kinase signaling resulting from specific genomic aberrations. (16) These aberrations are attractive therapeutic targets, as demonstrated by the pharmacologic inhibitor of BTK, ibrutinib, which blocks AML blast proliferation, migration, and leukemic cell adhesion to bone marrow stromal cells. (15) However, BTK-based treatment of AML patients has been unsuccessful to date, (22) with only a few pre-clinical, ex-vivo reports suggesting that ibrutinib is effective against FLT3(ITD) and CD117 harboring cells, unlike the clinical benefit seen in patients with CLL and lymphoma. (18, 21) Adding inhibitory pressure on the BTK pathway might enhance the efficacy of this strategy, as previously reported. (19, 20, 50-54) In this study, using a combination of genetic and biochemical approaches, we extensively characterize ARQ531, a novel, reversible, orally bioavailable, ATP-competitive inhibitor of BTK and associated kinases. ARQ531 greatly compromises AML cell survival by modulating transcriptional regulatory machinery coordinated by MYC, demonstrating activity both in-vitro and in a patient-derived xenograft (PDX) AML mouse model. Thus, our study provides rationale for developing clinical trials using ARQ531 as a new treatment for patients with AML.

Since ibrutinib does not directly inhibit members of the MAPK pathway, it is possible that the superior activity of ARQ531 in AML may be due to its modulation of additional targets, including kinases related to ERK signaling. (27) Although screening analysis of Src-family kinases (including Lyn and Syk) did not show any effect on AML cells, (55-57) (**Suppl. Fig.S10**) we assume that targeting of additional kinases is responsible for the high anti-AML activity of ARQ531. By combining

computational models and whole transcriptional analysis, we observed that ARQ531 treatment induces dysregulation of several transcription-addicted programs, including MYC and MYB. The combination of BTK inhibition and MYC/MYB downregulation explains the improved anti-AML activity of ARQ531 compared to single agent TKI's such as ibrutinib. Since ARQ531 simultaneously inhibits different cellular functions such as folding machinery, metabolic dependency, and genome integrity, it may provide deeper and more durable remissions, while delaying the emergence of resistance. Additionally, based on reports that degrading MYB eradicates AML cells in mice without impairing normal myelopoiesis, (46) ARQ531 treatment may be safe for hematopoietic precursors cells, supporting its clinical relevance. We also provide experimental evidence that the bone marrow stroma is not affected by treatment and, more importantly, does not affect ARQ531 anti-tumor activity. Preliminary phase 1 studies confirm the ARQ531 safety profile, adding to the data that support its clinical development.

Recent studies suggest that modulating transcriptional regulatory machinery is an innovative strategy to treat blood malignancies, including AML. (14, 38) An example of this strategy is all-trans retinoic acid (ATRA) treatment which, by modulating the transcriptional target PML-RARα, induces differentiation of leukemic blasts resulting in improved patients survival. (58) However, most transcription factors remain notoriously difficult to target, with siRNA-mediated silencing of gene expression being one of the few feasible approaches. (59) Other oncoproteins, including MYC and MYB, are emerging as compelling targets for drug development in AML, due to their ability to influence tumor proliferation. (40-44, 60, 61) In this context, the new small molecule ARQ531, by affecting multiple oncogenic pathways simultaneously, results in perturbation of the transcriptional regulatory machinery which maintains AML cell integrity. Therefore, targeting BTK, MYC and MYB with ARQ531 represents an innovative strategy for improving the efficacy of AML therapy.

In summary, we have demonstrated that ARQ531, a new reversible tyrosine kinases inhibitor, suppresses AML cells viability in vitro and in vivo by abrogating different oncogenic targets including BTK, MYC and MYB. Gene silencing of BTK, MYC and MYB in AML cells was not as effective as ARQ531, suggesting that other covalent or noncovalent targets are involved in its mechanism of action. Based on our preclinical data, we provide the rationale to explore the effects of this multi-targeted agent on hematologic malignancies as well as solid tumors, beyond investigating its clinical benefit in AML patients.

ACKNOWLEDGMENTS

This work was supported in part by the Associazione Italiana per la Ricerca sul Cancro (AIRC, MYFG #18491 to M.C. and # 21552 to A.C.; I.G. to F.B.), Italian Ministry of Health (5 x 1000 Funds of IRCCS San Martino-IST 2014 and 2015, to M.C. and A.C.), Associazione Italiana Leucemie Linfomi e Mieloma (AIL sezione di Genova) and University of Genoa, Italy

REFERENCES

1. Sant M, Allemani C, Tereanu C, et al. Incidence of hematologic malignancies in Europe by morphologic subtype: results of the HAEMACARE project. Blood. 2010;116(19):3724-3734.

2. Ferrara F, Schiffer CA. Acute myeloid leukaemia in adults. Lancet. 2013;381(9865):484-495.

3. Esposito MT, So CW. DNA damage accumulation and repair defects in acute myeloid leukemia: implications for pathogenesis, disease progression, and chemotherapy resistance. Chromosoma. 2014;123(6):545-561.

4. Stein EM. FLT3 inhibitors for relapsed or refractory acute myeloid leukaemia. Lancet Oncol. 2018;19(7):849-850.

5. El Fakih R, Rasheed W, Hawsawi Y, Alsermani M, Hassanein M. Targeting FLT3 Mutations in Acute Myeloid Leukemia. Cells. 2018;7(1).

6. DiNardo CD, Stein EM, de Botton S, Roboz GJ, et al. Durable Remissions with Ivosidenib in IDH1-Mutated Relapsed or Refractory AML. N Engl J Med. 2018;378(25):2386-2398.

7. Buggy JJ, Elias L. Bruton tyrosine kinase (BTK) and its role in B-cell malignancy. Int Rev Immunol. 2012;31(2):119-132.

8. Hendriks RW, Bredius RG, Pike-Overzet K, Staal FJ. Biology and novel treatment options for XLA, the most common monogenetic immunodeficiency in man. Expert Opin Ther Targets. 2011;15(8):1003-1021.

9. Herman SEM, Montraveta A, Niemann CU, et al. The Bruton Tyrosine Kinase (BTK) Inhibitor Acalabrutinib Demonstrates Potent On-Target Effects and Efficacy in Two Mouse Models of Chronic Lymphocytic Leukemia. Clin Cancer Res. 2017;23(11):2831-2341.

10. Wilson WH, Young RM, Schmitz R, et al. Targeting B cell receptor signaling with ibrutinib in diffuse large B cell lymphoma. Nat Med. 2015;21(8):922-926.

11. Advani RH, Buggy JJ, Sharman JP, et al. Bruton tyrosine kinase inhibitor ibrutinib (PCI-32765) has significant activity in patients with relapsed/refractory B-cell malignancies. J Clin Oncol. 2013;31(1):88-94.

12. Treon SP, Tripsas CK, Meid K, et al. Ibrutinib in previously treated Waldenstrom's macroglobulinemia. N Engl J Med. 2015;372(15):1430-1340.

13. Rushworth SA, Bowles KM, Barrera LN, Murray MY, Zaitseva L, MacEwan DJ. BTK inhibitor ibrutinib is cytotoxic to myeloma and potently enhances bortezomib and lenalidomide activities through NF-kappaB. Cell Signal. 2013;25(1):106-112.

14. Grommes C, Pastore A, Palaskas N, et al. Ibrutinib Unmasks Critical Role of Bruton Tyrosine Kinase in Primary CNS Lymphoma. Cancer Discov. 2017;7(9):1018-1029.

15. Rushworth SA, Murray MY, Zaitseva L, Bowles KM, MacEwan DJ. Identification of Bruton's tyrosine kinase as a therapeutic target in acute myeloid leukemia. Blood. 2014;123(8):1229-1238.

16. Oellerich T, Mohr S, Corso J, et al. FLT3-ITD and TLR9 use Bruton tyrosine kinase to activate distinct transcriptional programs mediating AML cell survival and proliferation. Blood. 2015;125(12):1936-1947.

17. Wu H, Hu C, Wang A, et al. Ibrutinib selectively targets FLT3-ITD in mutant FLT3-positive AML. Leukemia. 2016;30(3):754-757.

18. Rushworth SA, Pillinger G, Abdul-Aziz A, et al. Activity of Bruton's tyrosine-kinase inhibitor ibrutinib in patients with CD117-positive acute myeloid leukaemia: a mechanistic study using patient-derived blast cells. Lancet Haematol. 2015;2(5):e204-211.

19. Rotin LE, Gronda M, MacLean N, et al. Ibrutinib synergizes with poly(ADP-ribose) glycohydrolase inhibitors to induce cell death in AML cells via a BTK-independent mechanism. Oncotarget. 2016;7(3):2765-2779.

20. Li X, Yin X, Wang H, et al. The combination effect of homoharringtonine and ibrutinib on FLT3-ITD mutant acute myeloid leukemia. Oncotarget. 2017;8(8):12764-12774.

21. Pillinger G, Abdul-Aziz A, Zaitseva L, et al. Targeting BTK for the treatment of FLT3-ITD mutated acute myeloid leukemia. Sci Rep. 2015;5:12949.

22. Cortes JE EE, Stein AS, Graef T, et al. A multicenter, open-label phase 2a study of ibrutinib with or without cytarabine in patients with acute myeloid leukemia (PCYC-1131). J Clin Oncol. 2015;33(15_suppl):TPS7096-TPS7096.

23. Chong IY, Aronson L, Bryant H, et al. Mapping genetic vulnerabilities reveals BTK as a novel therapeutic target in oesophageal cancer. Gut. 2018;67(10):1780-1792.

24. Moyo TK, Wilson CS, Moore DJ, Eischen CM. Myc enhances B-cell receptor signaling in precancerous B cells and confers resistance to Btk inhibition. Oncogene. 2017;36(32):4653-4661.

25. Sun B, Shah B, Fiskus W, Qi J, Rajapakshe K, Coarfa C, et al. Synergistic activity of BET protein antagonist-based combinations in mantle cell lymphoma cells sensitive or resistant to ibrutinib. Blood. 2015;126(13):1565-1574.

26. Sasi BK, Martines C, Xerxa E, et al. Inhibition of SYK or BTK augments venetoclax sensitivity in SHP1-negative/BCL-2-positive diffuse large B-cell lymphoma. Leukemia. 2019;33(10):2416-2428.

27. Reiff SD, Mantel R, Smith LL, et al. The BTK Inhibitor ARQ 531 Targets Ibrutinib-Resistant CLL and Richter Transformation. Cancer Discov. 2018;8(10):1300-1315.

28. Lane SW, Scadden DT, Gilliland DG. The leukemic stem cell niche: current concepts and therapeutic opportunities. Blood. 2009;114(6):1150-1157.

29. Bam R, Ling W, Khan S, et al. Role of Bruton's tyrosine kinase in myeloma cell migration and induction of bone disease. Am J Hematol. 2013;88(6):463-471.

30. Chang BY, Francesco M, De Rooij MF, et al. Egress of CD19(+)CD5(+) cells into peripheral blood following treatment with the Bruton tyrosine kinase inhibitor ibrutinib in mantle cell lymphoma patients. Blood. 2013;122(14):2412-2424.

31. Zaitseva L, Murray MY, Shafat MS, et al. Ibrutinib inhibits SDF1/CXCR4 mediated migration in AML. Oncotarget. 2014;5(20):9930-9938.

32. Dhillon AS, Hagan S, Rath O, Kolch W. MAP kinase signalling pathways in cancer. Oncogene. 2007;26(22):3279-3290.

33. Lamba S, Russo M, Sun C, et al. RAF suppression synergizes with MEK inhibition in KRAS mutant cancer cells. Cell Rep. 2014;8(5):1475-1483.

34. McCubrey JA, Steelman LS, Franklin RA, et al. Targeting the RAF/MEK/ERK, PI3K/AKT and p53 pathways in hematopoietic drug resistance. Adv Enzyme Regul. 2007;47:64-103.

35. Sears R, Nuckolls F, Haura E, Taya Y, Tamai K, Nevins JR. Multiple Ras-dependent phosphorylation pathways regulate Myc protein stability. Genes Dev. 2000;14(19):2501-2514.

36. Sonenberg N, Hinnebusch AG. Regulation of translation initiation in eukaryotes: mechanisms and biological targets. Cell. 2009;136(4):731-745.

37. Zucal C, D'Agostino VG, Casini A, et al. EIF2A-dependent translational arrest protects leukemia cells from the energetic stress induced by NAMPT inhibition. BMC Cancer. 2015;15:855.

38. Brien GL, Valerio DG, Armstrong SA. Exploiting the Epigenome to Control Cancer-Promoting Gene-Expression Programs. Cancer Cell. 2016;29(4):464-476.

39. Li S, Vallet S, Sacco A, Roccaro A, Lentzsch S, Podar K. Targeting transcription factors in multiple myeloma: evolving therapeutic strategies. Expert Opin Investig Drugs. 2019;28(5):445-462.

40. Coulibaly A, Haas A, Steinmann S, Jakobs A, Schmidt TJ, Klempnauer KH. The natural anti-tumor compound Celastrol targets a Myb-C/EBPbeta-p300 transcriptional module implicated in myeloid gene expression. PLoS One. 2018;13(2):e0190934.

41. Ramaswamy K, Forbes L, Minuesa G, et al. Peptidomimetic blockade of MYB in acute myeloid leukemia. Nat Commun. 2018;9(1):110.

42. Xu Y, Milazzo JP, Somerville TDD, et al. A TFIID-SAGA Perturbation that Targets MYB and Suppresses Acute Myeloid Leukemia. Cancer Cell. 2018;33(1):13-28 e8.

43. Walf-Vorderwulbecke V, Pearce K, Brooks T, et al. Targeting acute myeloid leukemia by drug-induced c-MYB degradation. Leukemia. 2018;32(4):882-889.

44. Liu W, Wu M, Huang Z, et al. c-myb hyperactivity leads to myeloid and lymphoid malignancies in zebrafish. Leukemia. 2017;31(1):222-233.

45. Uttarkar S, Dasse E, Coulibaly A, et al. Targeting acute myeloid leukemia with a small molecule inhibitor of the Myb/p300 interaction. Blood. 2016;127(9):1173-1182.

46. Roe JS, Mercan F, Rivera K, Pappin DJ, Vakoc CR. BET Bromodomain Inhibition Suppresses the Function of Hematopoietic Transcription Factors in Acute Myeloid Leukemia. Mol Cell. 2015;58(6):1028-1039.

47. Zuber J, Shi J, Wang E, et al. RNAi screen identifies Brd4 as a therapeutic target in acute myeloid leukaemia. Nature. 2011;478(7370):524-528.

48. Filippakopoulos P, Qi J, Picaud S, et al. Selective inhibition of BET bromodomains. Nature. 2010;468(7327):1067-1073.

49. Pattabiraman DR, Gonda TJ. Role and potential for therapeutic targeting of MYB in leukemia. Leukemia. 2013;27(2):269-277.

50. Linley A, Krysov S, Ponzoni M, Johnson PW, Packham G, Stevenson FK. Lectin binding to surface Ig variable regions provides a universal persistent activating signal for follicular lymphoma cells. Blood. 2015;126(16):1902-1910.

51. Cea M, Cagnetta A, Acharya C, et al. Dual NAMPT and BTK Targeting Leads to Synergistic Killing of Waldenstrom Macroglobulinemia Cells Regardless of MYD88 and CXCR4 Somatic Mutation Status. Clin Cancer Res. 2016;22(24):6099-6109.

52. Deng J, Isik E, Fernandes SM, Brown JR, Letai A, Davids MS. Bruton's tyrosine kinase inhibition increases BCL-2 dependence and enhances sensitivity to venetoclax in chronic lymphocytic leukemia. Leukemia. 2017;31(10):2075-2084.

53. Hing ZA, Mantel R, Beckwith KA, et al. Selinexor is effective in acquired resistance to ibrutinib and synergizes with ibrutinib in chronic lymphocytic leukemia. Blood. 2015;125(20):3128-3132.

54. de Rooij MF, Kuil A, Kraan W, et al. Ibrutinib and idelalisib target B cell receptor- but not CXCL12/CXCR4-controlled integrin-mediated adhesion in Waldenstrom macroglobulinemia. Haematologica. 2016;101(3):e111-115.

55. Puissant A, Fenouille N, Alexe G, et al. SYK is a critical regulator of FLT3 in acute myeloid leukemia. Cancer Cell. 2014;25(2):226-242.

56. Hahn CK, Berchuck JE, Ross KN, et al. Proteomic and genetic approaches identify Syk as an AML target. Cancer Cell. 2009;16(4):281-294.

57. Dos Santos C, Demur C, Bardet V, Prade-Houdellier N, Payrastre B, Recher C. A critical role for Lyn in acute myeloid leukemia. Blood. 2008;111(4):2269-2279.

58. Lo-Coco F, Orlando SM, Platzbecker U. Treatment of acute promyelocytic leukemia. N Engl J Med. 2013;369(15):1472.

59. Yan C, Higgins PJ. Drugging the undruggable: transcription therapy for cancer. Biochim Biophys Acta. 2013;1835(1):76-85.

60. Mertz JA, Conery AR, Bryant BM, et al. Targeting MYC dependence in cancer by inhibiting BET bromodomains. Proc Natl Acad Sci U S A. 2011;108(40):16669-16674.

61. Zuber J, Rappaport AR, Luo W, et al. An integrated approach to dissecting oncogene addiction implicates a Myb-coordinated self-renewal program as essential for leukemia maintenance. Genes Dev. 2011;25(15):1628-1640.

TABLES

Table 1. AML patient characteristics

Patient	FAB classification	karyotype	NPM	FLT3-ITD	ELN RISK GROUP
AML-013	AML M2	normal	MUT	wt	low
AML-012	AML M1	normal	MUT	MUT	int.
AML-011	AML M6	complex	wt	wt	high
AML-009	AML M2	50XX	wt	wt	high
AML-007	AML M3	t(15;17)	/	wt	M3
AML-006	AML M4	normal	MUT	MUT	low
AML-005	AML M2	normal	MUT	MUT	low
AML-004	AML M4	normal	MUT	wt	low
AML-003	AML M2	normal	wt	wt	int
AML-001	AML M3	t(15;17)	/	MUT	M3
AML-008	AML M3	t(15;17)	/	wt	M3
AML-010	AML M4	n.a	wt	wt	int.
AML-002	AML M2	normal	MUT	wt	high

FIGURE LEGENDS

Figure 1. ARQ531 shows strong anti-tumor activity by inducing AML cells apoptosis. A) Immunoblot for phospho-BTK, BTK and GAPDH (loading control) in the indicated human AML cell lines and primary AML samples regardless of specific genomic landscape. **B, C)** Viability of AML cell lines after ARQ531 (B**)** or ibrutinib (C) treatment as measured by MTS assay. Displayed are the mean ± standard deviation (SD) from at least 3 independent experiments. **D)** IC_{50} values measured for each tested cell line as B and C. **E)** Drug effects on primary AML patient-derived samples (n=13) treated with increasing doses of ARQ531 or ibrutinib (0-30μM for 48 hours). IC50 values are visualized for each tested primary AML cell lines **F)** HL60, OCI-AML2 and primary AML-002 cells were treated with ARQ531 or DMSO (CTR) in a dose-dependent manner for 48 hours. Apoptotic cells were detected by Annexin V/PI staining. Representative dot plots are shown. **G)** Immunoblots for PARP, caspase 3, MCL-1, BCL-2 and tubulin on indicated AML cell lines and primary blast cells following BTK inhibitor treatment (ARQ531 vs ibrutinib) at 24 hours.

Figure 2. ARQ531 triggers anti-AML toxicity regardless of BTK activity and presence of stromal cells but preserves normal HSCs. A) Viability of OCI-AML2 GFP/luc+ cells treated with ARQ531 for 48 hours, alone and in presence of normal MSCs (blank) or AML-MSCs (grey) stroma, measured by luciferase-based luminescence assay. Data are represented as mean +/− SD in all histograms (n = 3). *0.02<p<0.03; **p < 0.05. **B-D)** Healthy donor (HD) derived hematopoietic precursor (BM-$CD34^+$) and PBMCs were exposed to increased doses of ARQ531, and clonogenic abilities (C) or viability (B, D) were calculated. Colony formation of ARQ531-treated cells (CFC) were measured after 2 weeks. Viability was calculated as propidium iodide-negative cells among CD34+ population. Data are represented as mean +/− SD (n = 3); unpaired t test, ***p < 0.001, ****p < 0.0001. **E)** Western blot showing that ARQ531 treatment effectively abrogates BTK signaling cascade in three different human

AML cell lines (HL60, OCI-AML3 and MOLM14) following 24 hours of treatment. Ibrutinib effect is also shown as a positive control. **F)** Viability of BTK-silenced (nucleofected with specific siRNAs targeting BTK) or control HL60 cells (siRNA scramble) treated with increasing doses of ARQ531 for 48 hours. Displayed are data represented as mean +/− SD in all (n = 3).

Figure 3. Molecular perturbation triggered by ARQ531 in AML cells. **A)** Heatmap for the highest 50 down- and up-regulated genes ($p < 0.0001$) following ARQ531 treatment of OCI-AML 3 cells. **B)** Volcano plot of RNA-seq of drug- versus DMSO-treated cells in OCI-AML3 showing that 377 and 852 genes were significantly up- and down-regulated, respectively, with a fold change (FC) > 2. **C)** Table of the ten most significantly enriched gene sets, from the Hallmark collection, enriched with genes downregulated by ARQ531 in AML cells. Number of genes in each set (n), the normalized enrichment score (NES), and test of statistical significance false discovery rate (FDR) q value are highlighted. **D)** Enrichment plots of top-four most significantly enriched gene sets (MYC-related) in transcriptional profiles of AML cells treated (right) or untreated (left) with ARQ531. **E)** Connectivity score generated by LINCS L1000 Characteristic Direction Signature Search Engine tool, that compared ARQ531-derived transcriptional profile against 10,000 "*perturbagen*" signatures (corresponding to short-hairpin RNA, open reading frame and compounds). Top-ranked scores of relevant results are indicated by arrow.

Figure 4. BTK inhibition and MYC/MYB degradation represent molecular basis for ARQ531 anti-AML activity. A) Western blot showing that 24h of ARQ531 (0.3-1 μM) treatment abrogates ERK and AKT activation in HL60 and OCI-AML2 cells. **B)** Western blot analysis shows that 24h of ARQ531 treatments (0.3-1 μM) affects kinases in the RAF/MEK/ERK pathway of AML cell lines, resulting in MYC-downregulation. **C**) Western blot showing time-dependent effects of ARQ531 exposure to p-MYC S62 and total MYC in HL60 cell line. **D**) Western blot showing deregulation of c-

MYC controlled signals in AML cells following treatment with ARQ531 at indicated doses following 24h. **E)** Viability of MYC-silenced or control HL60 cells treated with increasing doses of ARQ531 for 48 hours. Displayed are data represented as mean +/− SD in all (n = 3). **F)** Protein and mRNA expression in AML cells after 24 h treatment with DMSO or indicated ARQ531 concentrations, normalized to DMSO controls. Bars and error bars are means and SD of three independent experiments. *P<0.05; **P=0.01; ***P<0.001; n.s. not significant (relative to DMSO controls), one sample t-test. Western blots below graphs show examples of MYB protein expression. **G)** Western blot analysis of MYB protein expression in AML cells after 24 h treatment with DMSO, ARQ531 (0.3-1 μM) or ARQ531 and 10 μM MG132, a proteasome inhibitor.

Figure 5. ARQ531 treatment results in oncogenic program dysregulation in AML cells. A) Western blot analysis of ARQ531 (1 μM) treated cells after indicated hours. Time-dependent effects demonstrate early inhibition of BTK activity and MYC downregulation followed by MYB reduction with associated PARP and caspase 3 cleavage. **B)** Treatment of HL60 cells with BET bromodomain inhibitor JQ1 (400nM), ibrutinib (30 μM) or their combination which resulted in synergistic effect. Bars and error bars are means and SD of three independent experiments. ***P<0.001 (relative to DMSO controls), one sample t-test. **C)** Western blot showing that ibrutinib, JQ1, or the combination result in appearance of apoptotic features, including caspase 3 and PARP cleavage in HL60 cells

Figure 6. ARQ531 affects BTK, MYC and MYB in AML cells. A) BTK, MYC, MYB, and especially their simultaneous silencing considerably reduced viability of HL60 cells as measured by Typan blue staining. Displayed are the mean of triplicates. **B)** and **C)** Triple BTK/MYC/MYB silenced HL60 cells demonstrate diminished phosphorylation of ERK and PARP full length form compared with cells depleted either transiently **(B)** or stably **(C)** of each gene, individually.

Figure 7. ARQ531 inhibits tumor growth and extends survival in patient-derived xenograft (PDX) AML mouse model. A) Experimental outline for the analysis of the anti-leukemic activity of ARQ531 against primary human AML cells. Patient-derived xenograft mouse model of human primary AML cells was used to assess the efficacy of ARQ531 against AML cells isolated from patients with AML M4. B) Representative flow cytometric dot plots representing tumor engraftment evaluated at day 35 after treatment. On the right panel, histogram represents percentage of human CD45+ cells in mice. Data are represented as mean ± SD; **P=0.006; **** P<0.001. C) Circulating human CD45+ cells were measured in peripheral blood by flow cytometry weekly for 2 months. At day 19, a systemic xenograft was confirmed (tumor engraftment) and mice were randomized to receive vehicle control, ARQ531 low dose (25 mg/kg) or high dose (37.5 mg/kg). Percentage of human leukemic cells in peripheral blood of mice was measured weekly, up to day 42. ** 0.005< P <0.008. D) Kaplan-Meier curve of PDX AML-model following treatment with vehicle, ARQ531 at low dose (25 mg/kg) or high dose (37.5 mg/kg). Higher drug-schedule led to significant longer overall survival compared with vehicle-control treated mice (5 mice/group; p<0.001).

Figure 1

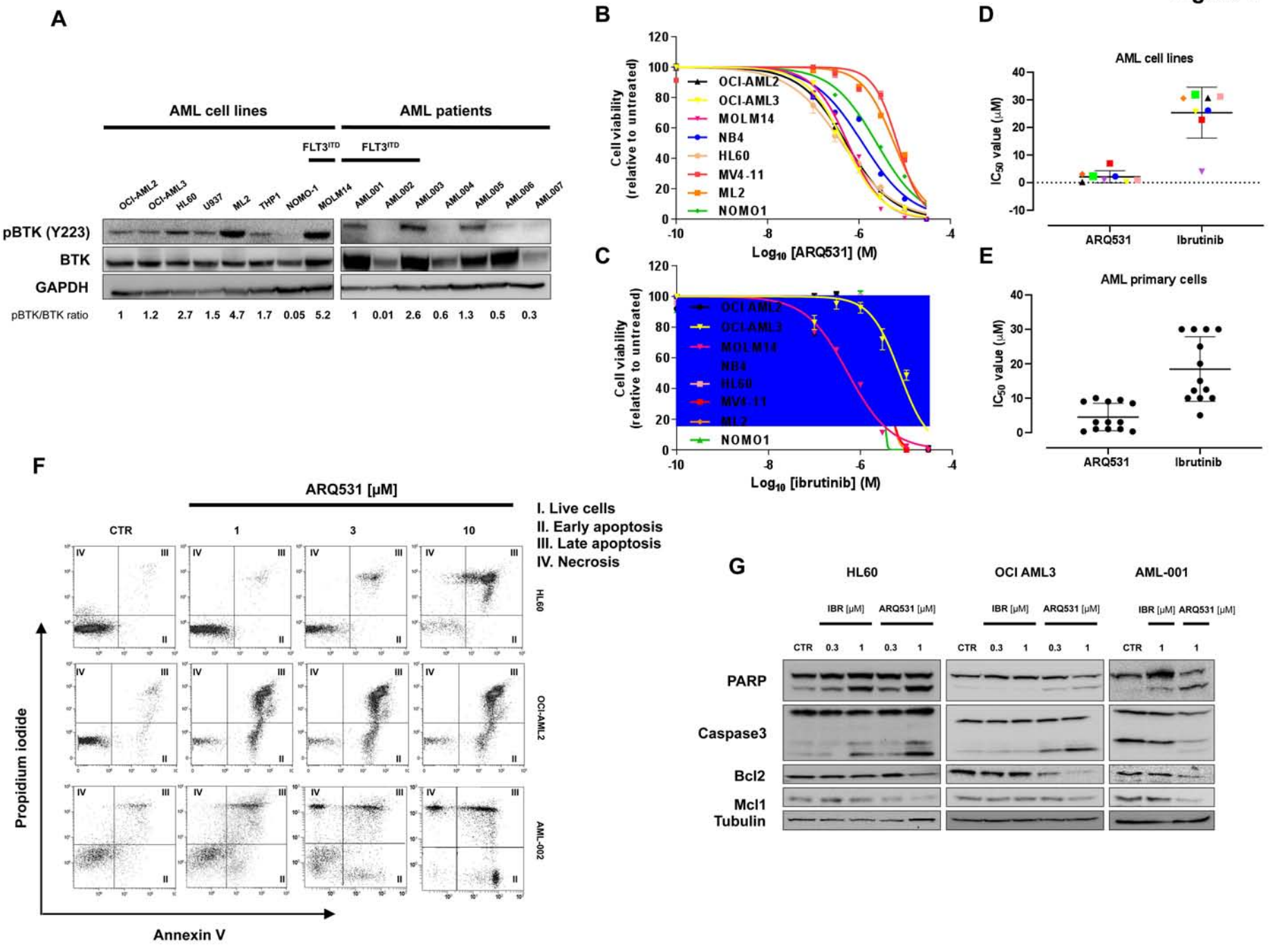
A
AML cell lines
AML patients
FLT3ITD
FLT3ITD
OCI-AML2
OCI-AML3
HL60
U937
ML2
THP1
NOMO-1
MOLM14
AML001
AML002
AML003
AML004
AML005
AML006
AML007
pBTK (Y223)
BTK
GAPDH
pBTK/BTK ratio
1 1.2 2.7 1.5 4.7 1.7 0.05 5.2 1 0.01 2.6 0.6 1.3 0.5 0.3
B
Cell viability (relative to untreated)
OCI-AML2
OCI-AML3
MOLM14
NB4
HL60
MV4-11
ML2
NOMO1
Log10 [ARQ531] (M)
C
Cell viability (relative to untreated)
Log10 [ibrutinib] (M)
D
AML cell lines
IC50 value (μM)
ARQ531
Ibrutinib
E
AML primary cells
IC50 value (μM)
ARQ531
Ibrutinib
F
ARQ531 [μM]
CTR
1
3
10
I. Live cells
II. Early apoptosis
III. Late apoptosis
IV. Necrosis
HL60
OCI-AML2
AML-002
Propidium iodide
Annexin V
G
HL60
OCI AML3
AML-001
IBR [μM]
ARQ531 [μM]
CTR 0.3 1 0.3 1
CTR 0.3 1 0.3 1
CTR 1 1
PARP
Caspase3
Bcl2
Mcl1
Tubulin

Figure 2

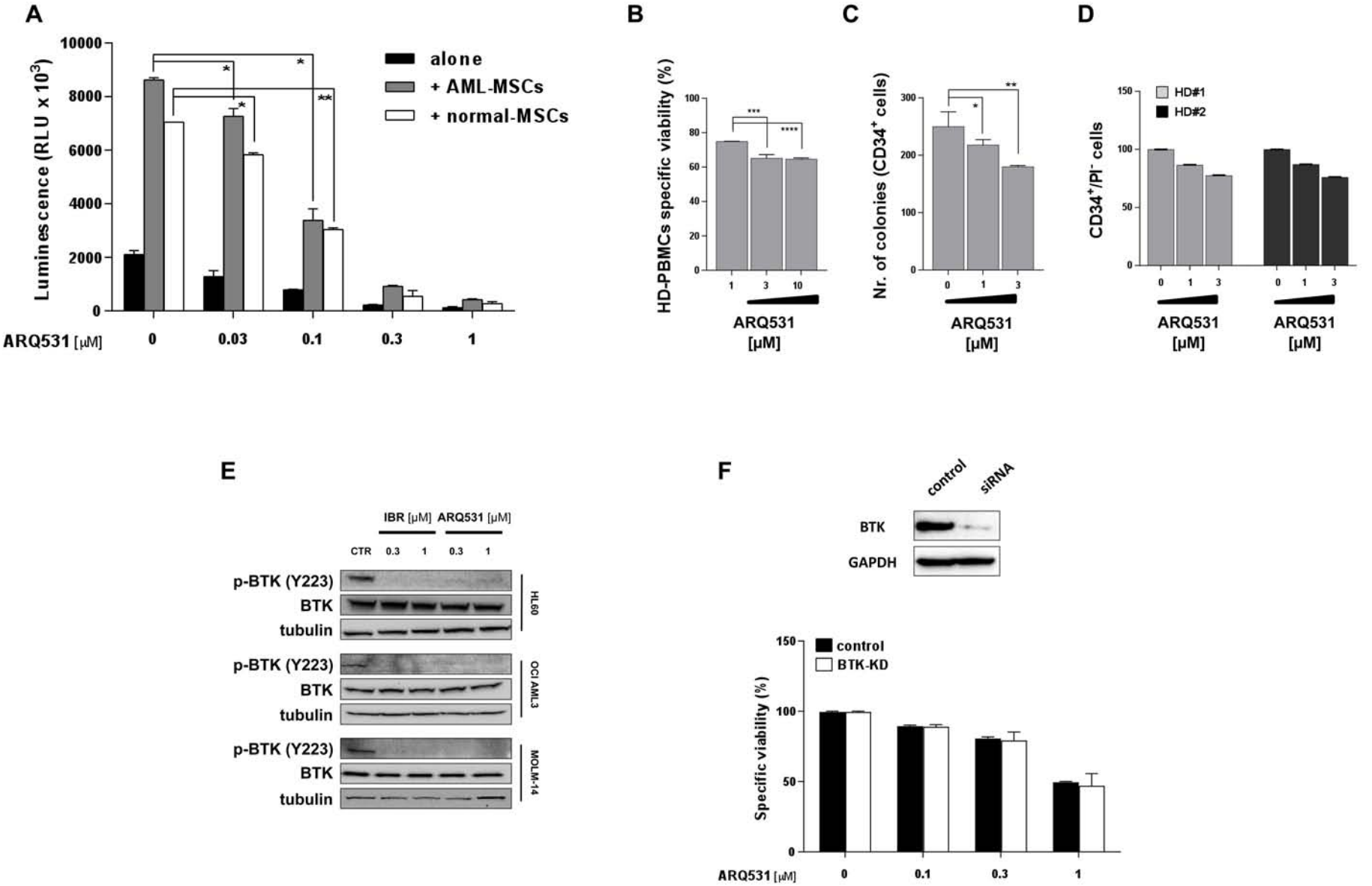
A
Luminescence (RLU x 10^3)
alone
+ AML-MSCs
+ normal-MSCs
ARQ531 [μM]
0
0.03
0.1
0.3
1
B
HD-PBMCs specific viability (%)
ARQ531 [μM]
C
Nr. of colonies (CD34+ cells)
ARQ531 [μM]
D
CD34+/PI- cells
HD#1
HD#2
ARQ531 [μM]
ARQ531 [μM]
E
IBR [μM]
ARQ531 [μM]
CTR
p-BTK (Y223)
BTK
tubulin
HL60
OCI AML3
MOLM-14
F
control
siRNA
BTK
GAPDH
control
BTK-KD
Specific viability (%)
ARQ531 [μM]

Figure 3

A

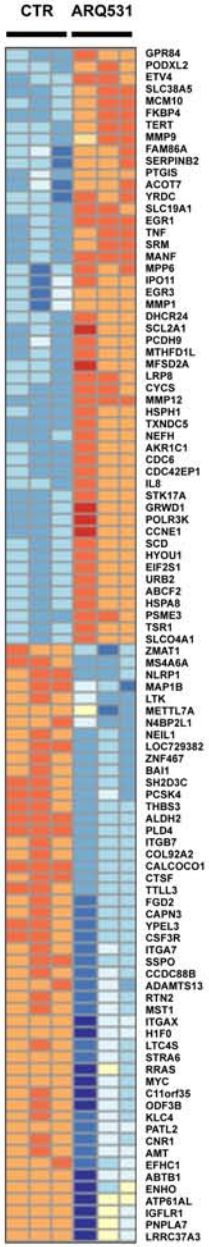

B

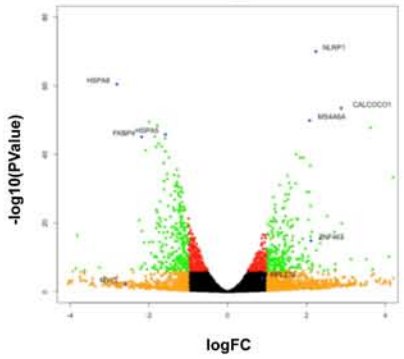

C

Top gene signatures

Gene Set	Size	ES	NES	FDR q-val
HALLMARK_MYC_TARGETS_V1	87	-0,48	-3,01	<0.0001
HALLMARK_MYC_TARGETS_V2	33	-0,61	-2,8	<0.0001
HALLMARK_MTORC1_SIGNALING	60	-0,49	-2,78	<0.0001
HALLMARK_UNFOLDED_PROTEIN_RESPONSE	26	-0,58	-2,54	<0.0001
MYC_UP.V1_UP	32	-0,61	-2,91	<0.0001
IL15_UP.V1_UP	23	-0,67	-2,85	<0.0001
KRAS.600.LUNG.BREAST_UP.V1_UP	12	-0,84	-2,81	<0.0001
IL2_UP.V1_UP	15	-0,76	-2,73	<0.0001
MTOR_UP.N4.V1_UP	20	-0,66	-2,64	<0.0001
RPS14_DN.V1_DN	27	-0,6	-2,64	<0.0001

D

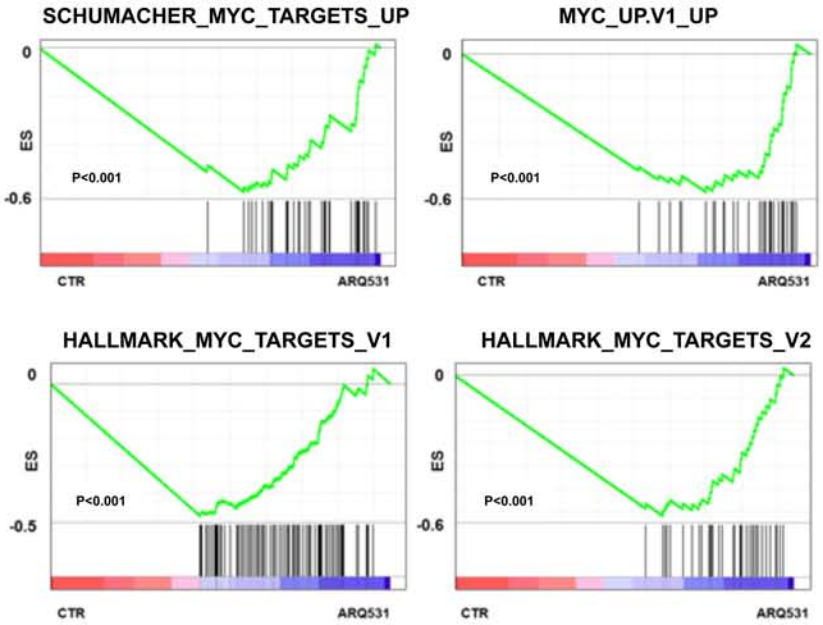

E

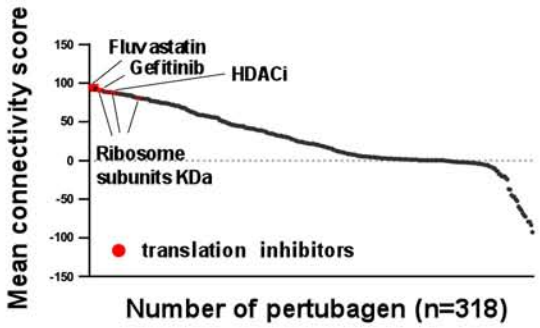

Figure 4

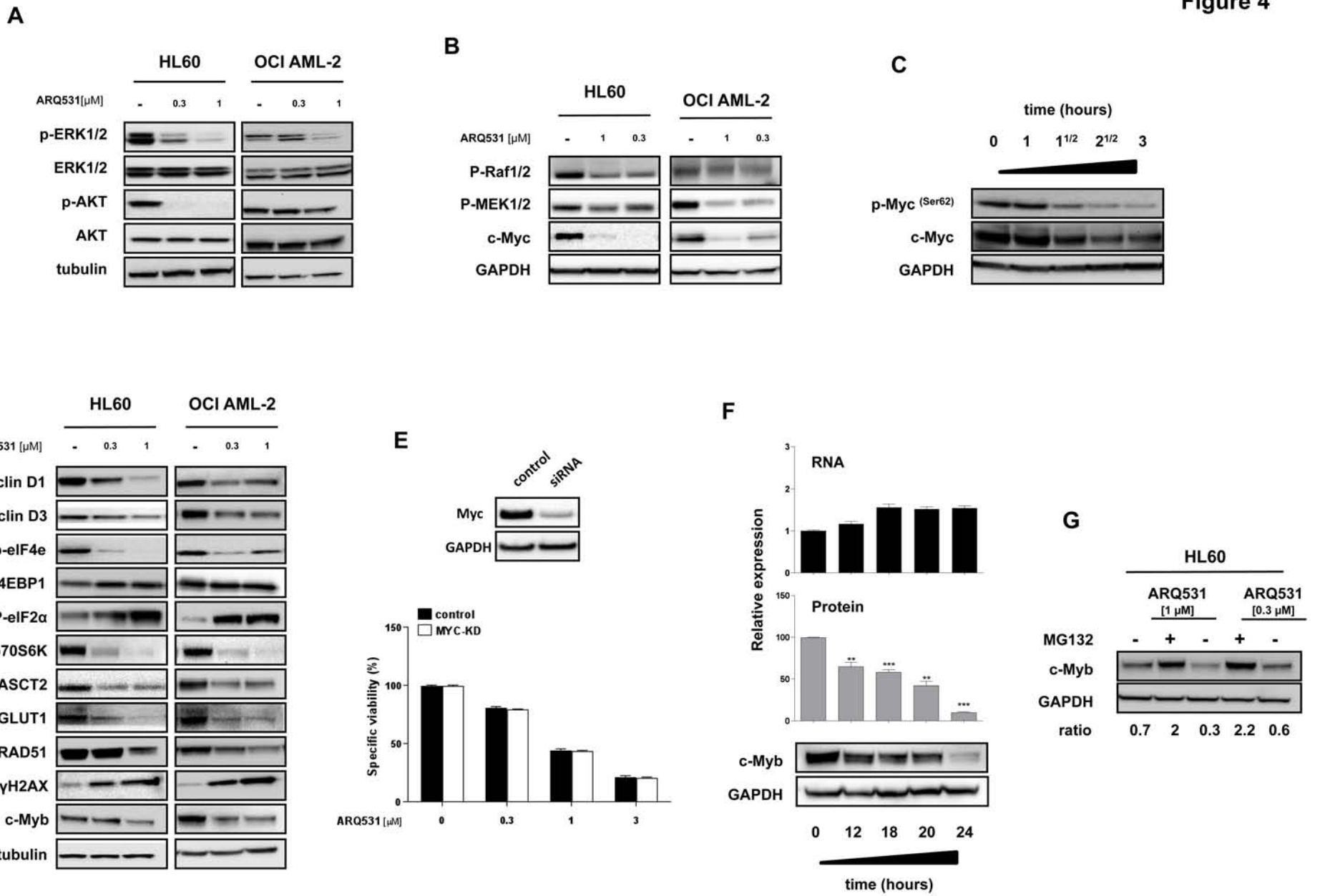
A
HL60
OCI AML-2
ARQ531[μM]
- 0.3 1 - 0.3 1
p-ERK1/2
ERK1/2
p-AKT
AKT
tubulin
B
HL60
OCI AML-2
ARQ531 [μM]
- 1 0.3 - 1 0.3
P-Raf1/2
P-MEK1/2
c-Myc
GAPDH
C
time (hours)
0 1 1^1/2 2^1/2 3
p-Myc (Ser62)
c-Myc
GAPDH
D
HL60
OCI AML-2
ARQ531 [μM]
- 0.3 1 - 0.3 1
Cyclin D1
Cyclin D3
p-eIF4e
4EBP1
P-eIF2α
pp70S6K
ASCT2
GLUT1
RAD51
p-γH2AX
c-Myb
tubulin
E
control
siRNA
Myc
GAPDH
control
MYC-KD
Specific viability (%)
150
100
50
0
ARQ531 [μM]
0 0.3 1 3
F
RNA
Relative expression
3
2
1
0
Protein
150
100
50
0
**
***
**
***
c-Myb
GAPDH
0 12 18 20 24
time (hours)
G
HL60
ARQ531 [1 μM]
ARQ531 [0.3 μM]
MG132
- + - + -
c-Myb
GAPDH
ratio
0.7 2 0.3 2.2 0.6

Figure 5

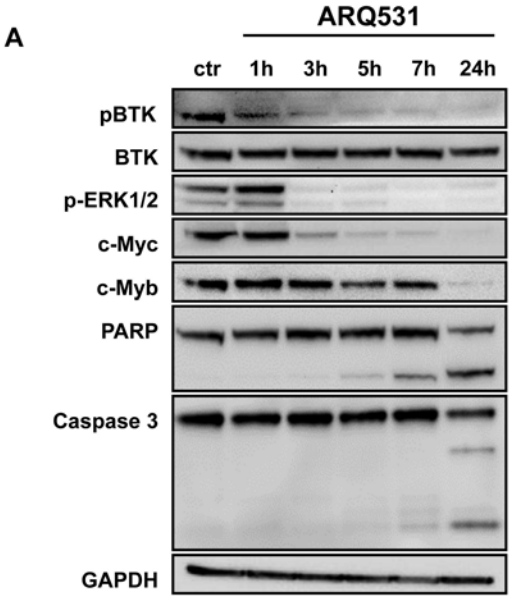
A
ARQ531
ctr
1h
3h
5h
7h
24h
pBTK
BTK
p-ERK1/2
c-Myc
c-Myb
PARP
Caspase 3
GAPDH

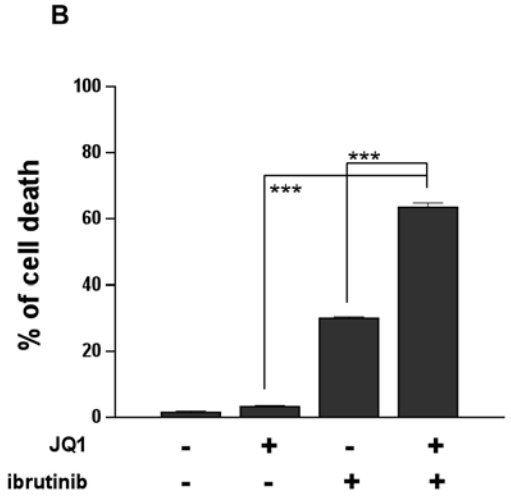
B
% of cell death
100
80
60
40
20
0
***
***
JQ1
ibrutinib
-
+
-
+
-
-
+
+

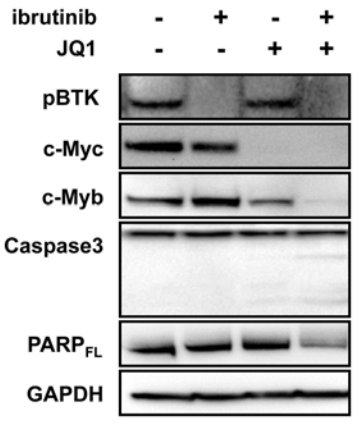
C
ibrutinib
JQ1
-
+
-
+
-
-
+
+
pBTK
c-Myc
c-Myb
Caspase3
PARP$_{FL}$
GAPDH

Figure 6

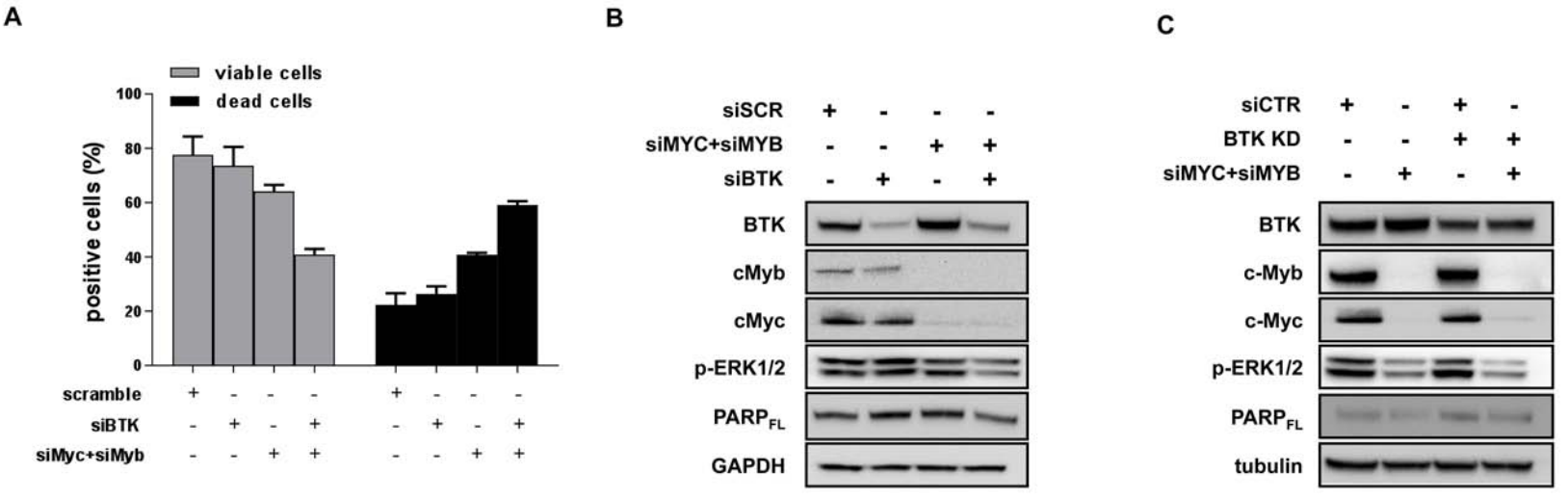
A
viable cells
dead cells
positive cells (%)
100
80
60
40
20
0
scramble + - - - + - - -
siBTK - + - + - + - +
siMyc+siMyb - - + + - - + +
B
siSCR + - - -
siMYC+siMYB - - + +
siBTK - + - +
BTK
cMyb
cMyc
p-ERK1/2
PARP FL
GAPDH
C
siCTR + - + -
BTK KD - - + +
siMYC+siMYB - + - +
BTK
c-Myb
c-Myc
p-ERK1/2
PARP FL
tubulin

Figure 7

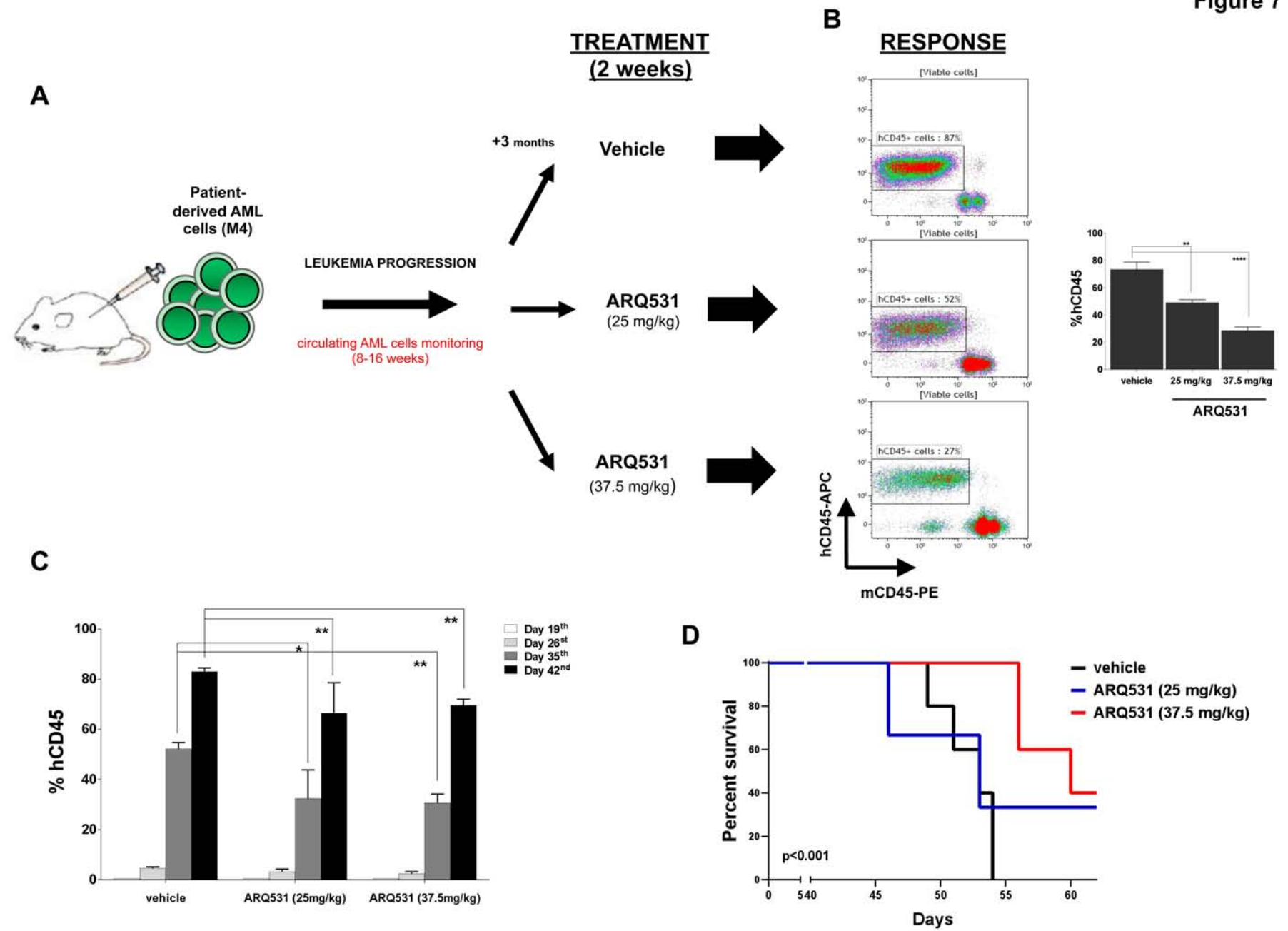
A
TREATMENT
(2 weeks)
B
RESPONSE
Patient-
derived AML
cells (M4)
LEUKEMIA PROGRESSION
circulating AML cells monitoring
(8-16 weeks)
+3 months
Vehicle
ARQ531
(25 mg/kg)
ARQ531
(37.5 mg/kg)
[Viable cells]
hCD45+ cells : 87%
hCD45+ cells : 52%
hCD45+ cells : 27%
hCD45-APC
mCD45-PE
%hCD45
vehicle
25 mg/kg
37.5 mg/kg
ARQ531
C
% hCD45
Day 19th
Day 26st
Day 35th
Day 42nd
vehicle
ARQ531 (25mg/kg)
ARQ531 (37.5mg/kg)
D
Percent survival
vehicle
ARQ531 (25 mg/kg)
ARQ531 (37.5 mg/kg)
p<0.001
Days

SUPPLEMENTAL EXPERIMENTAL PROCEDURES

Cell lines

The AML cell lines ML2, MOLM-14, MV4-11, HL60, NOMO-1, OCI-AML2, OCI-AML3 and NB4 were provided by collaborators or purchased from ATCC or DSMZ (Braunschweig, Germany). All cell lines were cultured in RPMI-1640 medium containing 10% FBS (GIBCO, Life Technologies, Carlsbad, CA), 2 μM l−1 glutamine, 100 U ml−1 penicillin, and 100 μg ml−1 streptomycin (GIBCO, Life Technologies, Carlsbad, CA). 293T cell line was purchased from ATCC and cultured in DMEM containing 10% FBS (GIBCO, Life Technologies, Carlsbad, CA), 4mM glutamine, 50 U ml/m1 penicillin, and 50 U/ml streptomycin (GIBCO, Life Technologies, Carlsbad, CA).

Primary cells

All studies involving human samples were performed under Policlinico San Martino Hospital (Genoa, Italy) IRB committee-approved protocols, after informed consent; de-identified samples were utilized. Primary leukemic cells were obtained from peripheral or bone marrow blood of 13 AML patients at diagnosis, before treatment. (Table 1) (1) The percentage of leukemic blasts was always > 90%. Normal $CD34^+$ cells (HSCs) were isolated from the bone marrow (BM) of healthy donors using anti-CD34 magnetic-activated microbeads and MiniMacs high-gradient magnetic separation column (Miltenyi Biotec, Bergisch Gladbach, Germany). This strategy generated highly purified $CD34^+$ cells (> 90%, as confirmed by FACS staining). Cells were either used immediately for viability assays or for mRNA isolation, or stored at −80°C in medium containing 50% FBS and 10% DMSO. Normal or AML MSCs, isolated as previously described, (2) were seeded in 96 well plates 1 × 104/well, AML cells were added to the confluent layer at 10:1 ratio. After overnight incubation, cells were used as indicated. Normal mononuclear cells (MNCs), obtained from the BM of healthy donors were isolated by Ficoll-Hypaque centrifugation (Amersham Bioscience, Piscataway, NJ, USA).

Cell Viability and Apoptosis Assay

Cell viability was assessed by using CellTiter 96 AQueous One Solution Cell Proliferation Assay (Promega Corporation, Madison, WI, USA), as previously described. (3) Apoptosis was evaluated by flow cytometric analysis following Annexin V–FITC (BD Biosciences, 556419) and PI (BD Biosciences, 51-6621E) staining, according to manufacturer's instructions. The percentage of cells undergoing apoptosis was defined as the sum of early apoptotic (annexin V+PI−) and late apoptotic (annexin V+PI+) cells.

RNA Seq processing, differentially expressed genes detection and gene set enrichment analysis

OCI-AML3 cells were treated with 1 μM ARQ 531 or vehicle control for 12 hours. RNA was prepared as mentioned earlier. A starting amount of 500 ng of RNA was used to prepare polyadenylate-enriched, single bar–coded libraries using the NEBNext Kit. Quality control of the libraries was evaluated by Bioanalyzer analysis with High Sensitivity chips (Agilent Technologies). Sequencing was performed on a HiSeq 2500 (Illumina) by 2× 50–base pair paired-end reads at the Biopolymers Facility of Harvard Medical School. We used Bcbio-next gen (https://github.com/bcbio/bcbio.nextgen/) to process the RNA-seq data. Briefly, *cutadapt* (https:// github.com/marcelm/cutadapt/) was used to trim adapters; trimmed reads were aligned to human reference genome (GRCh37) by tophat2; and read counts for each gene were calculated by HTSeq under standard parameters. Genes with low expression (fragments per kilobase million, FPKM, <1 across all samples) were filtered out. *Degust* (http://degust.erc.monash.edu/) was used for data visualization and differential analysis using *edgeR.* GSEA (https://software.broadinstitute.org/gsea/) was used on the pre-ranked gene lists, by applying 1000 permutations and using a weighted statistic enrichment. Significant enriched gene sets (16) were selected with a threshold FDR<0.25. Gene sets were downloaded from the Broad Institute's MSigDB (https://software.broadinstitute.org/gsea/msigdb/).

Western blotting

Whole-cell lysates were prepared as previously described. (3) Protein concentrations were determined by Bradford assay (Bio-Rad, CA), and equivalent amounts (40μg) were subjected to SDS-PAGE, transferred to PVDF membranes immunoblotted with following antibodies: anti-GAPDH (#5174, Cell Signaling Technology), -phospho-Histone H2A.X (Ser139) (#05-636, Millipore), -RAD51 (#588-B01P, Novus Biologicals), -Phospho-Btk (Tyr223) (#5082, Cell Signaling Technology), -BTK (#8547, Cell Signaling Technology), -γ tubulin (#MA1-850, ThermoFischer Scientific), -PARP (#9532, Cell Signaling Technology), -Caspase3 (#9662, Cell Signaling Technology), -Bcl2 (#sc-509, Santa Cruz Biotechnology), -Mcl1 (#sc-819, Santa Cruz Biotechnology), -Phospho-p44/42 MAPK (Erk1/2) (Thr202/Tyr204) (#4370, Cell Signaling Technology), -ERK1/2 (#9102, Cell Signaling Technology), Phospho-Akt (Ser473) (#4058, Cell Signaling Technology), AKT (#9272, Cell Signaling Technology), phospho-c-Raf (Ser338) (#9427, Cell Signaling Technology), phospho-MEK1/2 (Ser217/221) (#9154, Cell Signaling Technology), c-MYC (#9402, Cell Signaling Technology), Cyclin D1 (#2978, Cell Signaling Technology), Cyclin D3 (#2936, Cell Signaling Technology), Phospho-eIF4E (Ser209) (#9741, Cell Signaling Technology), Non-phospho-4E-BP1 (Thr46) (#4923, Cell Signaling Technology), Phospho-eIF2α (Ser51) (#3398, Cell Signaling Technology), Phospho-p70 S6 Kinase (Thr389) (#9206, Cell Signaling Technology), ASCT2 (#8057, Cell Signaling Technology), GLUT1 (#12939, Cell Signaling Technology), RAD51 (#sc-8349, Santa Cruz Biotechnology), c-MYB (clone 1-1) (#05-175, Millipore). Band intensities were quantified by Quantity One SW software (Bio-Rad Laboratories, Inc) using standard ECL Western Blotting Detection Reagents (Thermo Fisher Scientific, IL). Densitometric analysis of western blots was carried out using ImageJ software version 1.48 (National Institute of Health).

Lentiviral mediated gene transfer

pLV sh SCRAMBLE and pLV shBTK lentiviral vectors were purchased from Vector Builder (Vector Builder Inc., Santa Clara, USA) . For lentiviral transduction, 1×10^6 293T cells were plated on 60 mm Petri dishes and allowed to adhere for 24 h. Thereafter, cells were transfected with 1μg of lentiviral plasmidic DNA and 700ng of each of three packaging vectors (pRP CMV VSVG; pRP CMV gag:pol RRE; pRP CMV RSV Rev), using TransIT-293 (Mirus Bio, Madison, WI) according to the manufacturer's instructions. 48 and 72h after transfection, the supernatant containing lentiviral particles was harvested, filtered with a 0.45-μm-diameter filter, and used to infect 1.5×10^6 AML cells. AML cells were spinoculated at 750g for 45 min in presence of 8 μg ml−1 polybrene, (Santa Cruz Biotechnologies, CA), incubated with viral supernatant for 6 h and left overnight in normal culturing medium. The day after, a second cycle of infection was performed. Successfully infected cells were selected using a suitable concentration of puromycin (1 μg ml−1). 48 and 72 h after selection, the transduction efficiency was approximated by counting the proportion of cells expressing the fluorescent protein (GFP) using a fluorescence microscope (Nikon Eclipse 80i, Nikon, Melville, NY); and the knockdown efficiency was validated by protein level with WB analysis. Functional studies were performed as described below.

RNA Extraction and RT PCR.

Total RNA was extracted from cells using RNeasy Plus mini kit (Qiagen S.r.l., Milan, Italy) according to the manufacturer's instructions. 1 μg RNA was reverse transcribed in a final volume of 100 μl using High Capacity cDNA Reverse Transcription kit (Life Technologies, Monza, Italy). 5 μl of the resulting cDNA were used for qPCR with a QuantStudio5 Real-Time PCR (Applied Biosystems by Life Technologies, Monza, Italy). Primer sequences were as follows: MYB Fw 5'-CAAGCTCCGTTTTAATGGCAC-3', Rev 5'-ATCTTTCCACAGGATGCAGG -3' ; GAPDH Fw 5'-TCTCCTCTGACTTCAACAGCGAC-3', Rev 5'-CCCTGTTGCTGTAGCCAAATTC-3'. mRNA levels were detected using SYBR Select Master Mix (Applied Biosystems, Italy) according to the

manufacturer's protocol. Gene expression was normalized to housekeeping gene expression (GAPDH). Comparisons in gene expression were calculated using the $2^{-\Delta\Delta Ct}$ method.

Colony forming unit (CFU) assay

Immediately after their purification, $CD34^+$ HSCs were plated in HSC004 methylcellulose medium (R&D) supplemented with EPO 3 IU/ml and IL-6 20ng/ml at a concentration of $1x10^3$ cells per plate and treated (in duplicate) with different concentrations of ARQ531 or DMSO as control. All plates were incubated at 37°C, 5% CO2 for 10-14 days before counting the number of colonies.

BMSC conditioned media

10×10^5 Healthy donor- or Patient derived-BMSC were plated in 6 well plates and left to adhere for 24 hours. The day after, medium was replaced with 2 ml of complete RPMI-1640 and cells were cultured for 5 days. Thereafter, BMSC-conditioned media were collected, filtered with 0,45 µM filters and immediately used for AML cells resuspension. Finally, drugs or vehicle were added at 20X concentration, in order to not dilute conditioned media. After 48 hours cell viability was measured as indicated.

Tumor cell-specific bioluminescence imaging in co-cultures with stromal cells

$7x10^3$ $Luciferase^+$ AML cells (OCI-AML2 Plv sv40 GFP/luc+) were plated in 96-well optical white plates (Corning, Cat.No.3903) in the presence or absence of pre-plated $luciferase^-$ primary stromal cells (20×10^3 cells seeded 24hours before) and treated with drugs or veichle (DMSO), as indicated in each experiment. After 48 h of treatment, AML cell specific viability was assessed with Nano-Glo® Live Cell Assay System (Promega, Cat.No. N2011)

Nucleofection

HL60 cells were transfected by using the 4D-Nucleofector™ System (Lonza), according to manufacturer's instruction. Small interfering RNAs (siRNAs) targeting human BTK (ON-TARGET plus SMART pool, #L-003107-00-0005) and a non-targeting negative control (ON-TARGET plus non-

targeting pool #D-001810-10-05) were purchased from Dharmacon. siRNAs targeting human Myc or Myb were purchased from ThermoFisher Scientific (Myc siRNA#1 Dharmacon J-003282-23; Myb ThermoFisher Scientific #AM16708, pool of siRNA ID 115653 and 10768); #AM16708, pool of siRNA ID 115653 and 107687). For each nucleofection, 2 x 10^6 cells was pulsed with the EN-138 program, using Amaxa SF Cell line 4-D Nucleofector X KitL (Cat.No. V4XC-2024, Lonza). In this procedure, all siRNAs were used at the final concentrations of 500 nM. After 24h from nucleofection, cells were cultured and then treated or collected for further experiments.

Immunofluorescence and focal microscopy

Cells were prepared as previously described, (3) using specific primary and secondary antibodies. The slides were then mounted with ProLong Gold Antifade reagent (Invitrogen, Life Technologies, Carlsbad, CA), and images were taken using a Leica TCS SP confocal laser scanning microscope (Leica Microsystems, Wetzlar, Germany), equipped with 476, 488, 543 and 633 excitation lines with a 60 x Plan Apo oil objective.

Human Data Sets.

Expression levels of BTK were obtained from the TCGA cohort among their low or high expression of BTK. (BloodPortal data of BTK probe 205504_at from U133 Plus 2.0 array).

REFERENCES

1. Salvestrini V, Orecchioni S, Talarico G, Reggiani F, Mazzetti C, Bertolini F, et al. Extracellular ATP induces apoptosis through P2X7R activation in acute myeloid leukemia cells but not in normal hematopoietic stem cells. Oncotarget. 2016 Dec 13.

2. Ferrari D, Gulinelli S, Salvestrini V, Lucchetti G, Zini R, Manfredini R, et al. Purinergic stimulation of human mesenchymal stem cells potentiates their chemotactic response to CXCL12 and increases the homing capacity and production of proinflammatory cytokines. Exp Hematol. 2011 Mar;39(3):360-74, 74 e1-5.

3. Cagnetta A, Soncini D, Orecchioni S, Talarico G, Minetto P, Guolo F, et al. Depletion of SIRT6 enzymatic activity increases acute myeloid leukemia cells' vulnerability to DNA-damaging agents. Haematologica. 2018 Jan;103(1):80-90.

Supplementary Figure Legends.

Supplementary Figure 1. BTK expression in AML cells. BTK mRNA expression in AML as compared to other cancers, on the basis of data from The Cancer Cell Line Encyclopedia (CCLE) database. Data are presented as mean log2 expression with range; in red are highlighted AML cell lines (n=39).

Supplementary Figure 2. Anti-tumor activity of ARQ531 is dependent of caspase activation. A) HL60, OCI-AML2 and primary AML-004 cells were treated with increasing doses of ARQ 531 (1-10 μM) or DMSO for 48 hours. Apoptotic cell death was measured by Annexin V/PI staining and flow cytometric analysis. The percentage of each group is shown as solid columns. Data are derived from 3 independent experiments. **B)** HL60 cells were pretreated with caspase inhibitors (zVAD-fmk 50 μM), for 2 hours and then incubated with ARQ531 at indicated concentrations for 48 hours. Specific cell death was then measured with MTS assay.

Supplementary Figure 3. ARQ531 and Ibrutinib inhibit AML cell migration in response to SDF-1. HL60 cells were pretreated with ibrutinib (500nM) or ARQ531 (500nM) for 1 h before wash-off and then placed in the upper well of a 8.0μM transwell plate. The lower chamber contained 500ul of serum free media supplemented with SDF1 (100 ng/ml) for 3 hours and then assessed for cell number using trypan blue staining. Data were normalized to DMSO treated cells.*** p=.001; **** p<.0001

Supplementary Figure 4. Molecular perturbation triggered by ARQ531 in OCI-AML3 cells. A) Principal component analysis (PCA) of control and ARQ531 treatment on OCI-AML3 cells. **B)** GSEA analysis was performed on the entire set of signatures available from the Molecular Signatures Database (MSigDB). **C)** mRNA levels of selected genes were analyzed by qPCR in OCI-AML3 cell lines treated with 0.3 and 1 μM of ARQ 531 or ibrutinib for 24 hours. The graph shows the fold change compared to untreated cells.

Supplementary Figure 5. The pro-survival MAPK pathway has a crucial role for anti-AML activity of ARQ 531. A) HL60 cells were treated with increasing concentrations of ARQ531 w/w 20% FBS. After 24 hours, cells were collected for western blot analysis. In parallel viability was measured by MTS assay after 48 hours of drug exposure. **B)** HL60 cells treated with ARQ531 or Ibrutinib in presence or not of 20% FBS for 24h were subjected to blot analysis for phospho-ERK1/2, ERK1/2, c-Myc and tubulin as shown.

Supplementary Figure 6. ARQ531 treatment enhances genomic instability of AML cells. A) 3 x 10^6 HL60 cells were treated with ARQ531 for 24hours, using Doxorubicin as positive control. Thereafter, cells were washed with PBS, fixed and stained. γH2AX foci and nuclei (Q-nuclear) were visualized by confocal microscopy. **B)** 2 x 10^5 HL60 cells were plated in 96 well plate and treated for 48 hours with indicated doses of ARQ531 (0.3 μM) in presence or not of DNA damaging agents including idarubicin and Ara-C at indicated doses. Cell viability was than measured by MTS assay. Combination index was calculated by CalcuSyn software and reported above the columns indicating specific co-treatment. Data are represented as mean +/− SD in all histograms (n = 2). **0.01<p<0.05; ***p < 0.001.

Supplementary Figure 7. ARQ531 targets BTK and Myb in AML cells. A) Treatment of BTK-KD HL60 cells with increased doses of Mebendazole (0.2-1.8 μM) resulted in higher anti-AML activity of this drug. **B)** BTK, MYC/MYB, and especially triple gene knockdown considerably reduced viability of HL60 cells as measured by Typan blue staining. Displayed are the mean of triplicates.

Supplementary Figure 8. MYB and BTK expression highly correlate in AML patients. A) Microarray data from GSE13204 database are expressed as histogram plots (25th-75th percentiles) for BTK (A) and MYB (B) expression in AML patients (n = 542) and ND (n = 73). The data were log2 transformed and median centered (dark lines). C) Microarray gene expression data from GSE13204 data sets was robust multiarray average normalized and the correlation between BTK and MYB expression

in AML patients was assessed by the Spearman rank-order correlation, where $P < .05$ was considered as statistically significant.

Supplementary Figure 9. ARQ531 inhibits tumor growth in AML patient-derived xenograft (PDX) mice model. Tumor engraftment was determined by flow cytometry in bone marrow (BM) and spleen at day 53. Evaluated markers: human CD45. Any significant difference was observed among groups.

Supplementary Figure 10. ARQ531screening analysis on Src-family kinases. Immunoblots for CSK, FGR, HCK, YES, FYN, LCK pSRC and tubulin on OCI-AML3 cells following ARQ531 treatment at 24 hours at indicated doses.

A

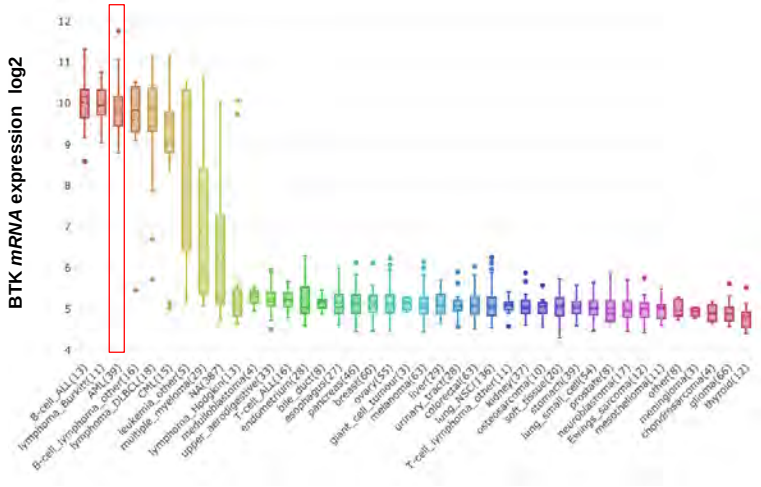
BTK mRNA expression log2
12
11
10
9
8
7
6
5
4
B-cell_ALL(13)
lymphoma_Burkitt(11)
AML(39)
B-cell_lymphoma_other(16)
lymphoma_DLBCL(18)
CML(15)
leukemia_other(5)
multiple_myeloma(33)
lymphoma_Hodgkin(13)
NAI(387)
medulloblastoma(3)
upper_aerodigestive(4)
T-cell_ALL(16)
endometrium(29)
bile_duct(8)
esophagus(27)
pancreas(46)
breast(60)
ovary(55)
giant_cell_tumour(3)
melanoma(63)
liver(23)
urinary_tract(29)
colorectal(67)
lung_NSCC(136)
T-cell_lymphoma_other(11)
kidney(37)
osteosarcoma(10)
soft_tissue(20)
stomach(38)
lung_small_cell(54)
prostate(9)
neuroblastoma(17)
Ewings_sarcoma(12)
mesothelioma(11)
other(9)
meningioma(31)
chondrosarcoma(4)
glioma(66)
thyroid(12)

Figure S2

A

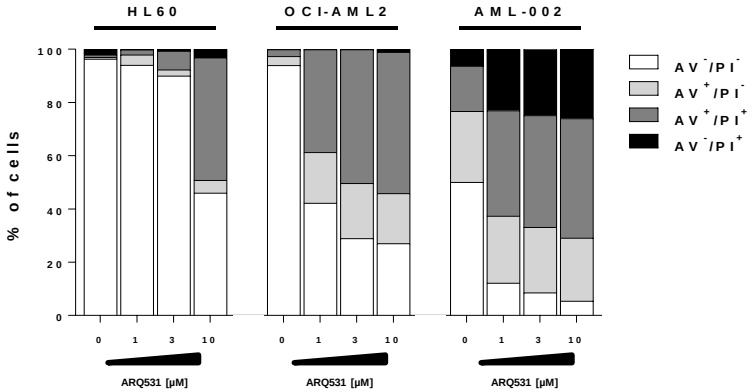
HL60
OCI-AML2
AML-002
% of cells
100
80
60
40
20
0
0 1 3 10
ARQ531 [µM]
AV-/PI-
AV+/PI-
AV+/PI+
AV-/PI+

B

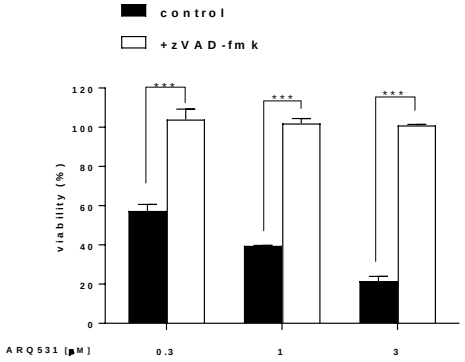
control
+zVAD-fmk
viability (%)
120
100
80
60
40
20
0
***
ARQ531 [µM]
0.3
1
3

Figure S3

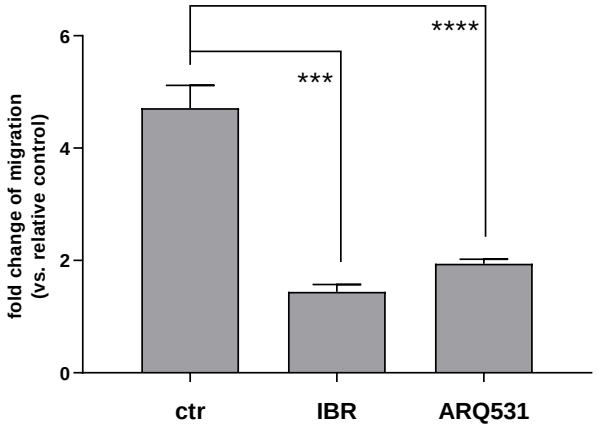
fold change of migration
(vs. relative control)
6
4
2
0
***
****
ctr
IBR
ARQ531

A

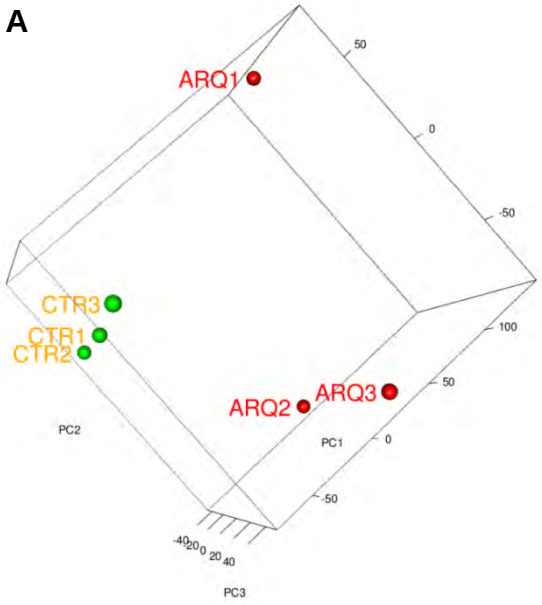

B

Myc-dependent Gene Set	Size	ES	NES	FDR q-val
SCHUHMACHER_MYC_TARGETS_UP	39	-0,59	-2,97	<0.0001
HALLMARK_MYC_TARGETS_V1	87	-0,48	-3,01	<0.0001
HALLMARK_MYC_TARGETS_V2	33	-0,62	-2,81	<0.0001
MYC_UP.V1_UP	32	-0,62	-2,91	<0.0001
WEI_MYCN_TARGETS_WITH_E_BOX	166	-0,56	-3,99	<0.0001
MENSSEN_MYC_TARGETS	31	-0,61	-2,81	<0.0001
DANG_MYC_TARGETS_UP	38	-0,51	-2,57	<0.0001
KIM_MYC_AMPLIFICATION_TARGETS_UP	34	-0,53	-2,51	<0.0001
SCHLOSSER_MYC_TARGETS_AND_SERUM_RESPONSE_DN	26	-0,56	-2,37	0,001
SCHLOSSER_MYC_TARGETS_REPRESSED_BY_SERUM	43	-0,46	-2,31	0,002

C

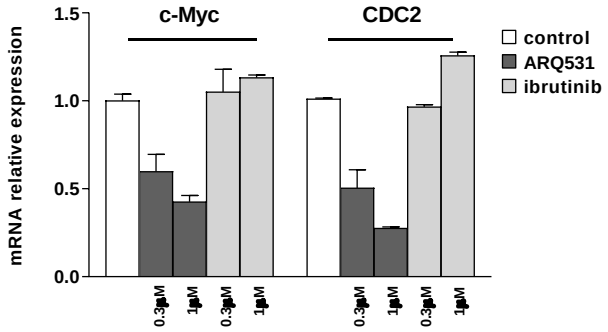

Figure S5

A

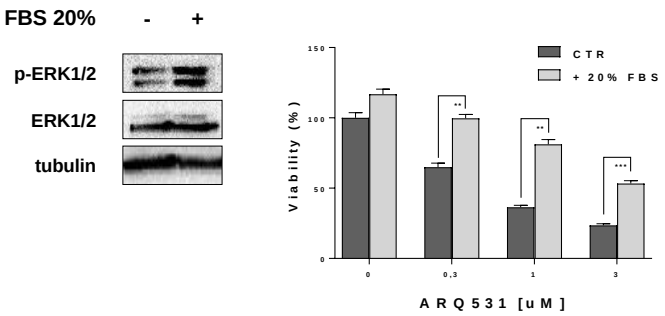
FBS 20%
-
+
p-ERK1/2
ERK1/2
tubulin
CTR
+ 20% FBS
Viability (%)
150
100
50
0
**
**
***
0
0,3
1
3
ARQ531 [uM]

B

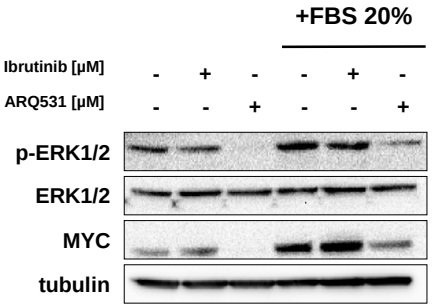
+FBS 20%
Ibrutinib [μM]
ARQ531 [μM]
- + - - + -
- - + - - +
p-ERK1/2
ERK1/2
MYC
tubulin

Figure S6

A

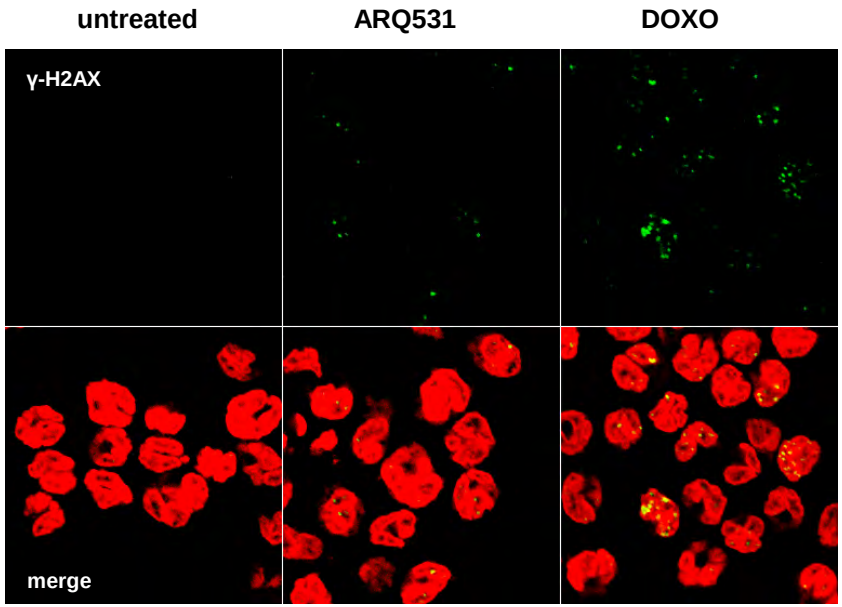
untreated
ARQ531
DOXO
γ-H2AX
merge

B

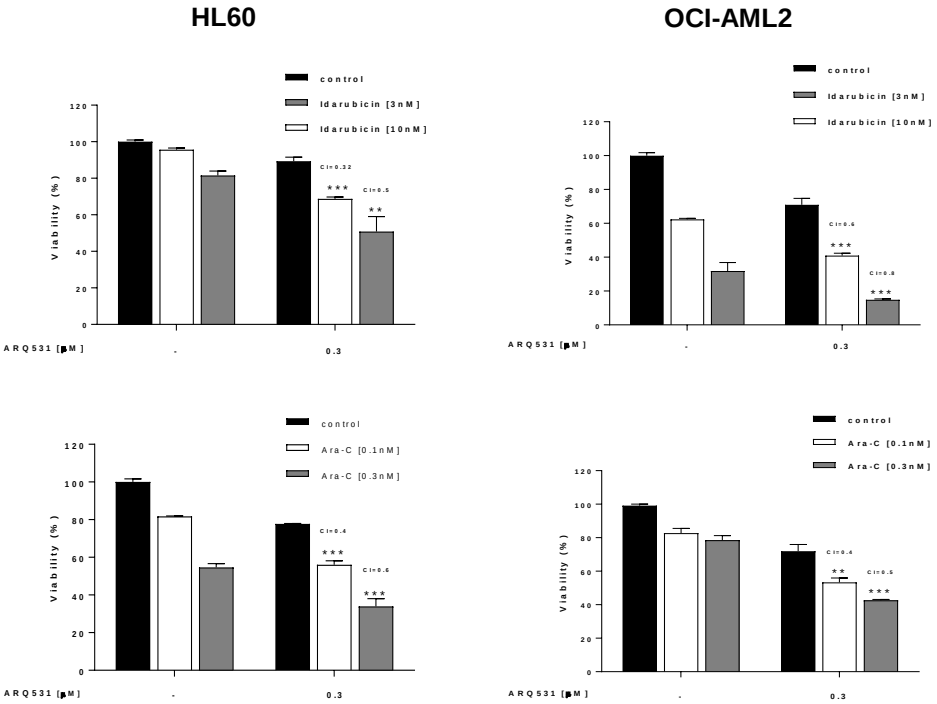
HL60
OCI-AML2
control
Idarubicin [3nM]
Idarubicin [10nM]
Ara-C [0.1nM]
Ara-C [0.3nM]
Viability (%)
ARQ531 [µM]
0.3

Figure S7

A

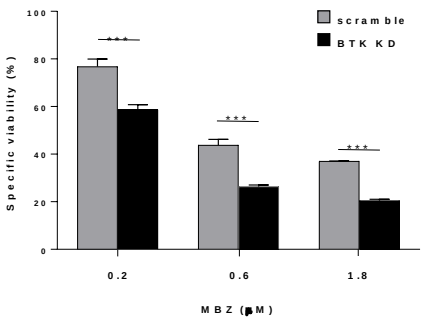
scramble
BTK KD
Specific viability (%)
100
80
60
40
20
0
***
***
***
0.2
0.6
1.8
MBZ (μM)

B

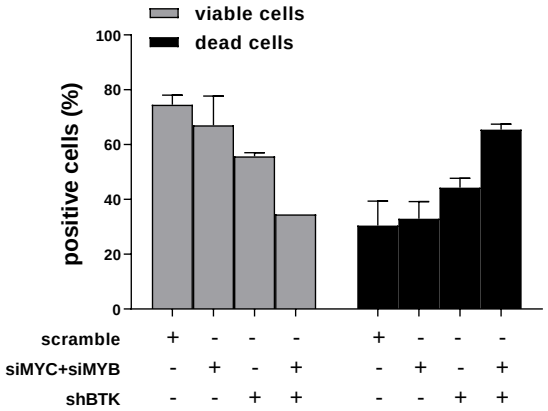
viable cells
dead cells
positive cells (%)
100
80
60
40
20
0
scramble + - - - + - - -
siMYC+siMYB - + - + - + - +
shBTK - - + + - - + +

Figure S8

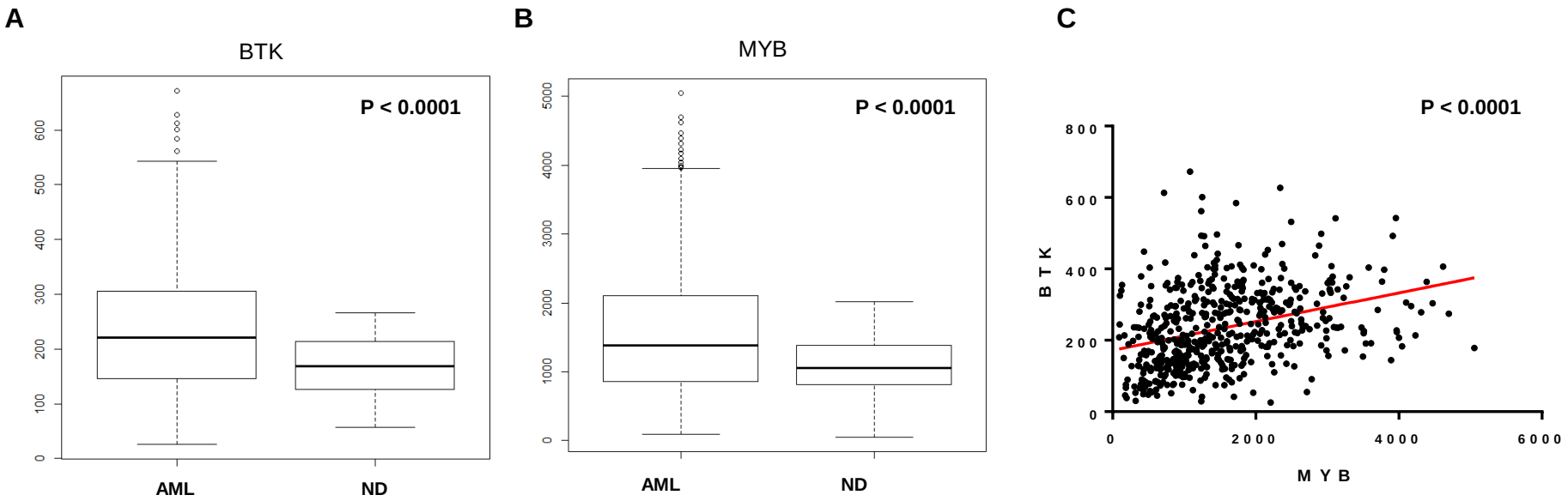
A
BTK
P < 0.0001
0
100
200
300
400
500
600
AML
ND
B
MYB
P < 0.0001
0
1000
2000
3000
4000
5000
AML
ND
C
P < 0.0001
BTK
0
200
400
600
800
MYB
0
2000
4000
6000

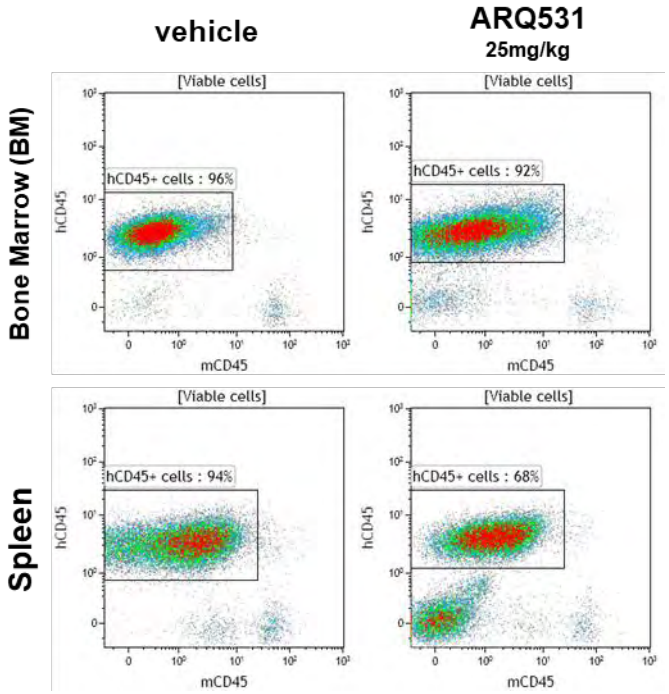
vehicle
ARQ531
25mg/kg
Bone Marrow (BM)
Spleen
[Viable cells]
hCD45+ cells : 96%
hCD45+ cells : 92%
hCD45+ cells : 94%
hCD45+ cells : 68%
hCD45
mCD45

Figure S10